Journal of African Earth Sciences 97 (2014) 143–160

Contents lists available at ScienceDirect

Journal of African Earth Sciences

journal homepage: www.elsevier.com/locate/jafrearsci

Relationships between deformation and magmatism in the Pan-African Kandi Shear Zone: Microstructural and AMS studies of Ediacaran granitoid intrusions in central Bénin (West Africa)

L. Adissin Glodji [a,b], J. Bascou [b,*], S. Yessoufou [a], R.-P. Ménot [b], A. Villaros [b]

[a] Département des Sciences de la Terre, Université d'Abomey-Calavi, 01 BP 526 Cotonou, Benin
[b] Université de Lyon, Université Jean Monnet and UMR-CNRS 6524, Laboratoire Magmas et Volcans, 42023 Saint Etienne, France

ARTICLE INFO

Article history:
Received 10 October 2013
Received in revised form 17 February 2014
Accepted 17 April 2014
Available online 30 April 2014

Keywords:
West Africa
Bénin-Nigerian Shield
Kandi shear zone
High-K calk-alkaline and alkaline granites
Microstructures
AMS

ABSTRACT

Relationships between the metamorphic basement, granitic intrusions and the Kandi Shear Zone (KSZ) in central Bénin have been investigated using petrological and structural approaches, in order to better understand the space and time parameters of the Pan-African shear deformation and the Ediacaran magmatism. In central Bénin, metamorphic rocks from the KSZ display a steep to vertical N–S trending foliation, a sub-horizontal mineral lineation together with kinematic indicators in agreement with a dextral transcurrent mega-shear zone. Four granitic intrusions (Dassa, Tré, Gobada and Tchetti) show many petrological similarities. They are biotite ± amphibole – ilmenite ± magnetite monzogranites with ferrous and metaluminous I-type features derived from high-K calk-alkaline magma. A fifth intrusion (Fita) is an alkali-feldspar, biotite, magnetite and ilmenite bearing granite crystallized from an alkaline magma. Moreover, high K_2O, Zr, Y, Nb and low CaO, MgO and Al_2O_3 contents together with high (FeOt/MgO) and low LIL/HFS elements ratios suggesting an A-type granite affinity.

Microstructural and AMS investigations presented in this paper show (i) solid-state deformation evidence for Dassa pluton and (ii) a magmatic deformation for the Tré, Tchetti, Gobada and Fita granitoids. Foliation in Dassa is parallel to the mesoscopic planar mylonitic foliation of the metamorphic basement. In the Tré, Tchetti, Gobada and Fita granitoids, magmatic textures and magnetic fabrics are coherent with the KSZ activity. These data suggest (i) a syn-kinematic nature for most of the intrusions (Tré, Gobada, Tchetti and Fita), except Dassa which correspond to an earlier event (ii) the succession of high-K calk-alkaline (Dassa, Tré, Gobada, Tchetti) evolves toward alkaline magmas (Fita) during the KSZ strike-slip tectonics. These observations highlight the changing nature of magma composition, magmatic processes and the different sources during KSZ activity in the Bénin Nigerian Shield. These new results suggest that the previous geodynamic interpretations, which assume a post-tectonic emplacement for the Gobada intrusion or an active continental margin setting for most of the late Pan-African (Ediacaran) granites intruded in central Bénin, has to be re-examined.

1. Introduction

The Bénin basement (Fig. 1a) belongs to the Neoproterozoic Pan-African Dahomeyides belt that results from the continental collision between the converging West African craton, Congo craton and East Sahara block during the assembly of Western Gondwana around 600 Ma ago (Ajibade and Wright, 1989; Affaton et al., 1991; Castaing et al., 1993; Trompette, 1994; Dada, 2008 and references therein). The Dahomeyides belt is a section of the larger Pan-African/Brasiliano belt (or Trans-Saharan orogenic belt, Liégeois et al., 2013) which stretches from North Africa to Northeast Brazil (Fig. 1a; Caby et al., 1991). Numerous transcontinental shear zones occur along the Pan-African/Brasiliano belt among which the Kandi Shear Zone (KSZ) extending from the Hoggar mountains (the so-called "4°50′ shear zone") and Dahomeyides belt in Africa to Northeast Brazil ("the Transbrasiliano lineament") (Caby, 1989; Trompette, 1994; Neves, 2003; Arthaud et al., 2008; Dos Santos et al., 2008). In the Dahomeyides belt, the KSZ has been active during the Neoproterozoic and successively reactivated during the Palaeozoic and Mesozoic (Guiraud and Alidou, 1981; Konate, 1996).

The late stage of the Pan-African/Brasiliano orogeny is characterized by emplacement of high-K calk-alkaline and alkaline

* Corresponding author. Tel.: +33 0 477485124; fax: +33 0 477485108.
E-mail address: jerome.bascou@univ-st-etienne.fr (J. Bascou).

http://dx.doi.org/10.1016/j.jafrearsci.2014.04.012
1464-343X/

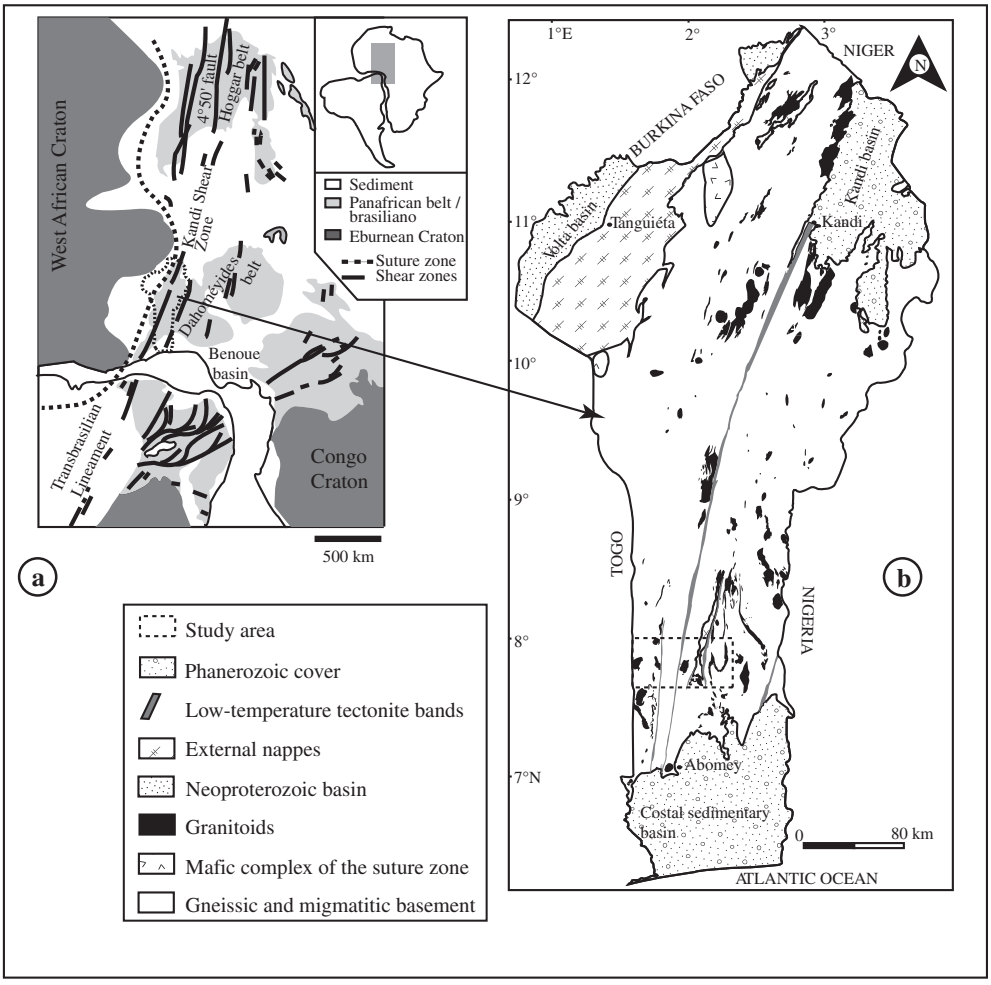

Fig. 1. Kandi Shear Zone extension; (a) through West Africa and North-Eastern Brazil before the South Atlantic Ocean opening (after Caby et al., 1991); (b) within the Bénin basement pointing out the close association in space of the Kandi Shear Zone, the plutonic and volcanic rocks.

granites. Different types of granites have been recognized; some are in association with thrust-related discontinuities while other are in association with syn- to late-transcurrent shear zones (e.g., Neves et al., 2000; Caby, 2003; Attoh et al., 2013; Dawai et al., 2013; Nsifa et al., 2013).

Granitic intrusions and volcanic rocks are associated to the KSZ in the western part of the Bénin-Nigerian shield of the Dahomeyides belt (Fig. 1b). On a structural point of view, granitic intrusions in the area were regarded as "isotropic" because of the absence of visible mesoscopic-scale structures. This way, without any detailed microstructural study and fabric analysis, these intrusions have been considered as post-tectonic bodies (Breda, 1989; Bigiorggero et al., 1988). Thus, detailed investigations on the magnetic mineral fabric have to be carried out in order to resolve the apparent "isotropy" of granitic intrusions.

The anisotropy of magnetic susceptibility (AMS) is a powerful tool to constrain the time relationship between granite emplacement and regional deformation. Such an approach has been applied in the Hoggar (Djouadi et al., 1997; Henry et al., 2007, 2009; Nouar et al., 2011), West and Central Africa (Ferré et al., 1995, 1997; Déléris et al., 1996; Dawai et al., 2013; Nsifa et al., 2013) and North-East Brazil (Archanjo et al., 1999, 2008, 2009; Neves et al., 1996, 2005).

This paper focuses on the petrological features and magnetic fabrics within the granitic intrusions associated to the KSZ in central Bénin. In that region, the Bénin-Nigerian basement is characterized by the close association of high-grade gneisses, migmatitic gneisses and granites as well as low-grade metavolcanic and metasedimentary units (c.f. Idaho-Mahou basin). Mineral chemistry and whole-rock chemistry are used to determine a preliminary genetic typology of the different granite compositions. The close association of magmatic and tectonic structures provides the opportunity to study the time relationship between tectonic movement and plutonic intrusions associated with the KSZ. Following the interpretation of petrological and geochemical data, an AMS study is used to determine the magnetic fabric, to understand the origin of the various granites formed in the region and to determine their relationship with the KSZ evolution.

2. Geological setting

The study area, located in the Central region of Bénin (Fig. 1b), consists of a crystalline basement built up by various gneisses of both granulite and amphibolite facies, by migmatites and by several granitoids. This basement is overlain by weakly metamorphic volcanic and sedimentary formations restricted to a narrow tectonic basin, the so-called Idaho-Mahou basin (Boussari and Rollet, 1974; Breda, 1989) (Fig. 2).

According to Breda (1989), the main granulite formation displays biotite + hypersthene + garnet parageneses. It is surrounded by amphibolite facies gneisses, migmatites and subordinate bands

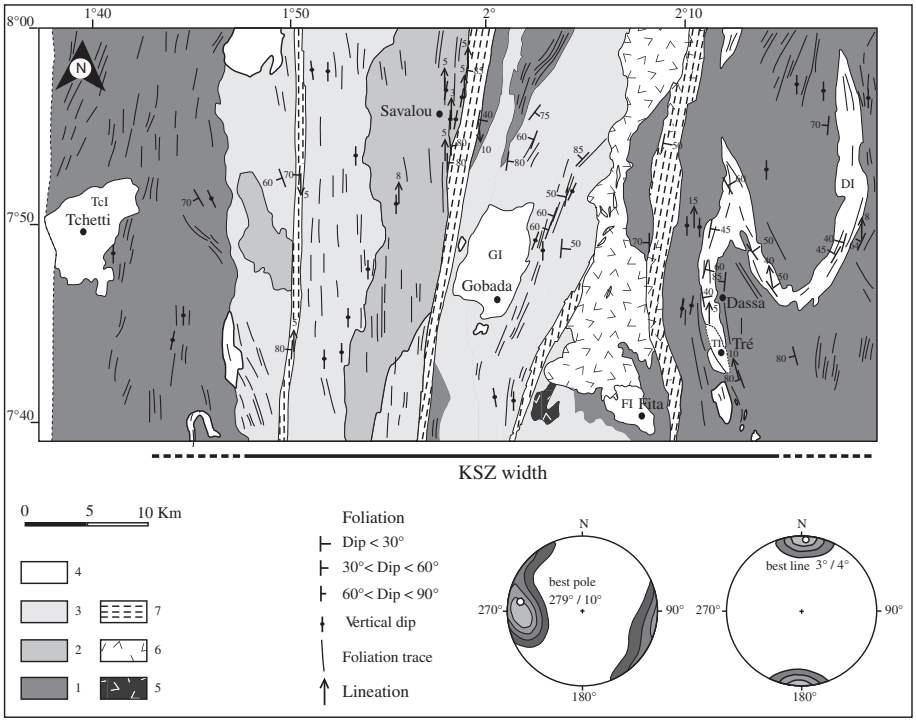

Fig. 2. Geological and structural map of the Kandi Shear Zone in central Bénin simplified from the 1:200,000 geological map of Breda (1989); (1) migmatites; (2) granulites and charnockites; (3) amphibolite facies gneisses; (4) granitoid intrusions; (5) metabasites; (6) volcano-sedimentary rocks of Idaho-Mahou basin; (7) late low-temperature tectonite bands. The estimated lateral extension of the Kandi Shear Zone is indicated by the horizontal solid and dotted line. Lower hemisphere, equal area projections of the pole of mesoscopic-scale foliations and lineations measured in the metamorphic rocks.

of marbles and quartzites. Amphibolite facies gneisses contain scarce relics of granulitic mineralogical assemblages and include various size bodies of charnockites (Breda, 1989). The mesoscopic foliations of gneisses and migmatites in the study area dip vertically with a meridian trend. Three N–S trending mylonitic bands of 1–3 km width crosscut the studied area and affect every rocks formations of the region. They are associated with retromorphic recrystallizations in greenschist facies conditions. These low temperature tectonites are parallel to the faults that delimit the Idaho-Mahou basin and correspond to the late activity of the KSZ. Very few radiometric data on the basement gneisses and migmatites are available. Whole-rock Rb–Sr ages of 1214 ± 117 Ma on the biotite–garnet gneisses and of 916 ± 69 Ma on the migmatites have been reported to the successive late Mesoproterozoic to early Neoproterozoic high grade metamorphic events (granulitic and anatectic) recorded by the crystalline basement (Breda, 1989). A 441 ± 5 Ma (K-Ar on muscovites) obtained on the greenschist facies mylonitic bands was considered to date the late kinematic of the KSZ (Breda, 1989).

Granite intrusions, spatially associated with the KSZ in central Bénin have been described by previous studies (Bessoles and Trompette, 1980; Bigiorggero et al., 1988 and Breda, 1989). Mainly based on field observations, different granite types have been recognized with regard to their texture and fabric. This way, regional granites can either be porphyritic (meta-)granite or looking as isotropic granite (Fig. 2). The Dassa intrusion is the only example of porphyritic granite. It occurs as a N–S lenticular body concordant with the surrounding migmatitic gneisses foliation and is affected by mega-scale open folds. Granite of the Dassa intrusion is amphibole + biotite bearing with sub-alkaline affinities and is mainly crust-derived (Bigiorggero et al., 1988). The apparent isotropic intrusions (Gobada and Fita granites) are biotite-bearing and display respectively sub-alkaline and alkaline affinities (Bessoles et Trompette, 1980; Bigiorggero et al., 1988). More specifically, the Fita granite is believed to be derived from both juvenile mantle and old crustal sources (Kalsbeek et al., 2012) and to end the plutonic suite in this area (Bigiorggero et al., 1988).

Very few radiometric data are available in the literature for Dassa, Gobada and Fita granitoids, but they all suggest a late Neoproterozoic age. Whole rock Rb/Sr data provide 620 ± 47 Ma (corrected from Caen-Vachette, 1975 with $I_{Sr} = 0.7119$ by Breda (1985)) and 579 ± 5 Ma (Caen-Vachette, 1975) respectively for Dassa and Fita while K-Ar data on biotite (Breda, 1985) gave younger ages, 523 ± 6 Ma and 521 ± 6 Ma respectively for Dassa and Gobada. In regard with the apparent isotropic fabric of the Gobada granite, the 521 Ma age has been commonly interpreted as the emplacement age and the intrusion viewed as post-dating the latest tectonic events of the Dahomeyides Pan-African belt (Breda, 1989).

The Idaho-Mahou volcano-sedimentary basin opened within the crystalline basement. It is N–S trending and about 100 km in length and width up to 10 km. According to Boussari and Rollet (1974) and Breda (1989), the basin is filled with metavolcanic rocks (basalts and rhyolites) and metasediments (conglomerates, sandstones, silts) and intruded by microgranite and fine-grained gabbros. All these rocks underwent metamorphic greenschists facies conditions in late Neoproterozoic.

3. New field and petrographic data

Recent field observations and petrological studies (Adissin Glodji, 2012) highlight new results concerning the metamorphic basement and the granitic intrusions.

3.1. The Paleo- to Mesoproterozoic metamorphic basement

As previously mentioned both granulitic and amphibolitic facies gneisses constitute the metamorphic basement. The latter of

Paleo- to Mesoproterozoic age underwent a very strong shearing during Neoproterozoic times in relation with the KSZ activity. Such deformation occurred under high and low temperature conditions and is marked by pervasive and vertical mylonitic foliations and by narrow cataclastic bands, which correspond to the previously denominated "mylonitic bands" of Breda (1989).

Typical granulites of the Savalou formation are two pyroxenes and garnet–biotite bearing gneisses. The recrystallization of orthopyroxene phenoclasts into lepidoblastic Bt–Qz assemblages marks out a retromorphic evolution from granulitic to upper amphibolite conditions. Finally, the presence of chlorite suggests a second retromorphic evolution from amphibolite to greenschists facies conditions.

Two different gneisses have been recognized: amphibole (pargasite) ± biotite ± garnet ± pyroxene gneiss and garnet ± biotite ± sillimanite ± cordierite aluminous gneiss. Both of them may locally record evidence for a very intensive partial melting, which leads to the formation of a large volume of migmatites. Gneisses and migmatites include numerous bodies and layers of various materials: amphibolites, amphibolo-pyroxenites, marbles, quartzites and the so-called charnockites (Breda, 1989). The latter are two pyroxenes and hornblende–biotite bearing rocks and they correspond to grano-monzodioritic intrusive protoliths, emplaced in granulitic conditions and later re-equilibrated in amphibolite facies metamorphism. These charnockites may represent relics of an earlier granulitic stage prior to the pervasive retrogression.

High-temperature mylonitic foliation generally trends N–S with a dip oscillating from 50° W and E to sub-vertical (Fig. 2; Fig. 3a and b). Mylonitic foliation planes bear sub-horizontal to horizontal (<30°) mineral stretching lineation defined by elongation of quartz and feldspar and by alignment of pyroxenes and amphiboles in granulites and amphibole–biotite gneisses respectively. Mesoscopic-scale folds affect the amphibolite facies gneisses and the migmatites. The axial planes of these folds trend NNW–SSE to NNE–SSW, i.e. parallel to the regional mylonitic foliation and are steeply plunging northwards (45–70°). In the same way, N–S and conjugate NNW–SSE trending shear bands of centimetric to metric scale can also be observed in the amphibolite facies gneisses and migmatites. These shear bands may locally collect leucosomes suggesting that shear zone development and melting are coeval. In the migmatites, leucosomes and late quartz veins are also boudinaged and slightly folded. This indicates that the deformation keeps going after the partial melting stage.

Shear criteria are abundant in the gneisses and migmatites. The most common kinematic indicators are asymmetrical recrystallized tails on feldspars porphyroclasts, asymmetrical pressure shadows on garnet porphyroclasts, rolling structures, S-C structures and asymmetrical lenses. These kinematic indicators consistently suggest a dextral shearing sense. Low-temperature tectonite bands (cataclastic bands) display sub-vertical to strongly dipping mylonitic foliation (Fig. 3c and d) and horizontal stretching lineation.

In summary, the occurrence of steep to vertical foliations and of sub-horizontal mineral lineations together with dextral kinematic indicators of the high-temperature mylonites are in agreement with the development of a large dextral transcurrent shear zone, which could reach fifty kilometers wide. Later deformation at lower temperatures is more spatially localized and forms the narrow, kilometric-scale cataclastic shear bands (Fig. 2).

3.2. Granitic intrusions

Five intrusions have been selected for detailed investigations: Dassa, Tré, Gobada, Tchetti and Fita (Fig. 2). All of them are located within the KSZ.

3.2.1. The tectonically deformed Dassa metagranite

The composite Dassa metagranite was sheared on a regional scale to form an elongate pluton as a "Z" shape fold defined by two N–S trending eastern and western flancs and a central NW–SE segment (Fig. 2). The Dassa deformed pluton consisted originally of granite and quartz-monzonite with porphyritic coarse-grained texture (Fig. 3e and f) crosscut by decimetric to decametric dykes of porphyritic medium-grained, biotite–muscovite microgranite emanating from the Tré intrusion. The quartz-monzonites occur as decametric-scale bodies within the granite.

Trends of the internal foliation of granite and quartz-monzonite, within the Dassa intrusion, are N–S in the western and eastern flancs and NNW–SSE and N–S in the central segment. The foliation dips steeply (45–60°) to the East in the western and central flancs and to the West in the eastern flanc of the intrusion. The mineral lineation is locally defined by sub-horizontal (10–40°), shape-preferred orientation of feldspar megacrysts. In the southern curvature of the intrusion, metric to decametric-scale folds are observed and the axial planes of these folds are parallel to the mylonitic foliation of country rocks gneisses and their axes are strongly plunging. At the margin of the intrusion, granites may be more strongly deformed and occur as porphyroclastic orthogneiss where recrystallization tails of feldspar porphyroclasts reveal a dextral sense of shearing (Fig. 3f).

The granite and quartz-monzonite of the Dassa intrusion are mostly composed of quartz, megacrystic K-feldspar, andesine and biotite. The quartz-monzonite contains additional amphibole. Accessory phases are abundant as apatite, allanite, titanite, zircon and ilmenite in these two facies and magnetite occurs in the quartz-monzonite. The mafic microgranular enclaves (MME) of Dassa intrusion are composed of plagioclase, biotite, amphibole, apatite, zircon, titanite and opaque minerals. They also enclose feldspars xenocrysts inherited from the host granite and quartz-monzonite during mingling processes (Fig. 3e). The magmatic assemblages are later partially replaced by syn-kinematic parageneses in successively amphibolite (KFsp2-Pl2-Bt2-Ttn2) and greenschists (Chl) facies conditions.

At the microscopic scale, K-feldspar and amphibole porphyroclasts together with large microfractured sheets of biotites are embedded within a grano-lepidoblastic matrix of fine-grained crystals of biotite, quartz and feldspars (andesine and K-feldspar) (Fig. 4a and b). Feldspar porphyroclasts are affected by successive ductile and brittle deformation with lamellae and later microfractures. They also display "core and mantle" structures or recrystallize into myrmekitic and secondary feldspars. Amphibole porphyroclasts show evidence of brittle deformation and crystallization of chlorite along microfractures. Quartz is affected by plastic deformation and recrystallization; it occurs as elongated phenoclasts with undulose extinction and as polycrystalline ribbons. A dextral sense of shearing is confirmed by asymmetrical recrystallized tails of feldspar porphyroclasts (Fig. 4b).

All these microstructures are consistent with solid-state deformation under amphibolite facies metamorphic conditions. The granites and quartz-monzonites of Dassa intrusion have been affected by dextral shearing after solidification.

3.2.2. The Tré, Gobada, Tchetti and Fita granites

The common structural criteria of these four granite intrusions are the quasi absence of visible fabrics on the field and the presence of mafic MME with lobate contours suggesting the lack of solid-state deformation (Fig. 3g). Furthermore, some decimetric to metric-scale rafts of the Dassa metagranite appear within the Tré granite (Fig. 3h) at the margins of the Tré intrusion. This clearly indicates that the intrusion of the Tré granite postdates the tectonic event, which deformed the Dassa pluton.

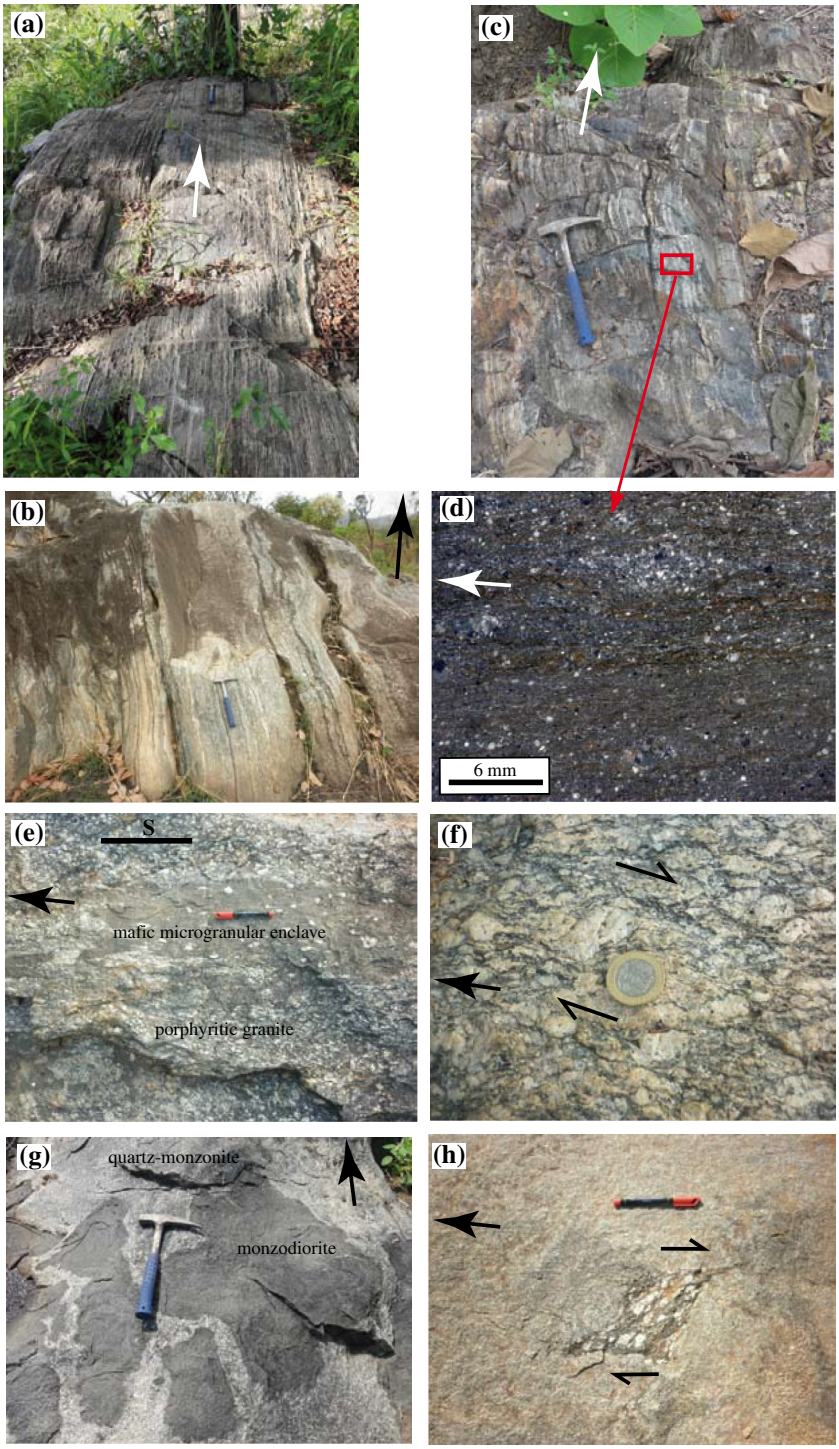

Fig. 3. Examples of outcrops in the Kandi Shear Zone. (a) Vertical N–S trending mylonitic foliation in granulites; (b) vertical N–S trending mylonitic foliation in migmatites (East area); (c) vertical mylonitic foliation in the low-temperature kilometric-scale shear bands; (d) focus on the low-temperature tectonite showing a fine-grained crushed and schistose cataclasite made of quartz, K-feldspar, biotite and muscovite; (e) porphyritic coarse-grained granite of Dassa intrusion with deformed mafic microgranular enclave (MME); (f) K-feldspar porphyroclasts in the deformed coarse-grained (meta-) granite of Dassa intrusion indicating a dextral shear sense; (g) oriented elongated enclaves of monzodiorite in the quartz-monzonite of the Gobada intrusion; (h) enclave of Dassa metagranite within the Tré granite showing the relative chronology of two intrusions. The full arrows indicate the North direction; the smaller half arrows indicate the shear sense; the line indicates the orientation of the foliation (S).

Locally, a weak magmatic foliation can be observed in the Tré and Gobada intrusions. This foliation is always oriented N–S and is displayed by preferred orientation of alkali feldspar phenocryst in the Tré granite, by biotite schlieren structures, and by the orientation of elongated monzodiorite enclaves respectively in the granite and the quartz-monzonite of the Gobada pluton (Fig. 3g).

3.2.2.1. The Tré, Gobada and Tchetti intrusions. These intrusions mainly consist of subalkaline to calk-alkaline granites, but the outcrops include less differentiated rocks such monzonite in Tré and monzogranite at Gobada. The granites are mostly composed of quartz, K-feldspar (Or_{100}), plagioclase (Ab_{100}) and biotite with additional muscovite (less than 5%) in the Tré and Tchetti facies.

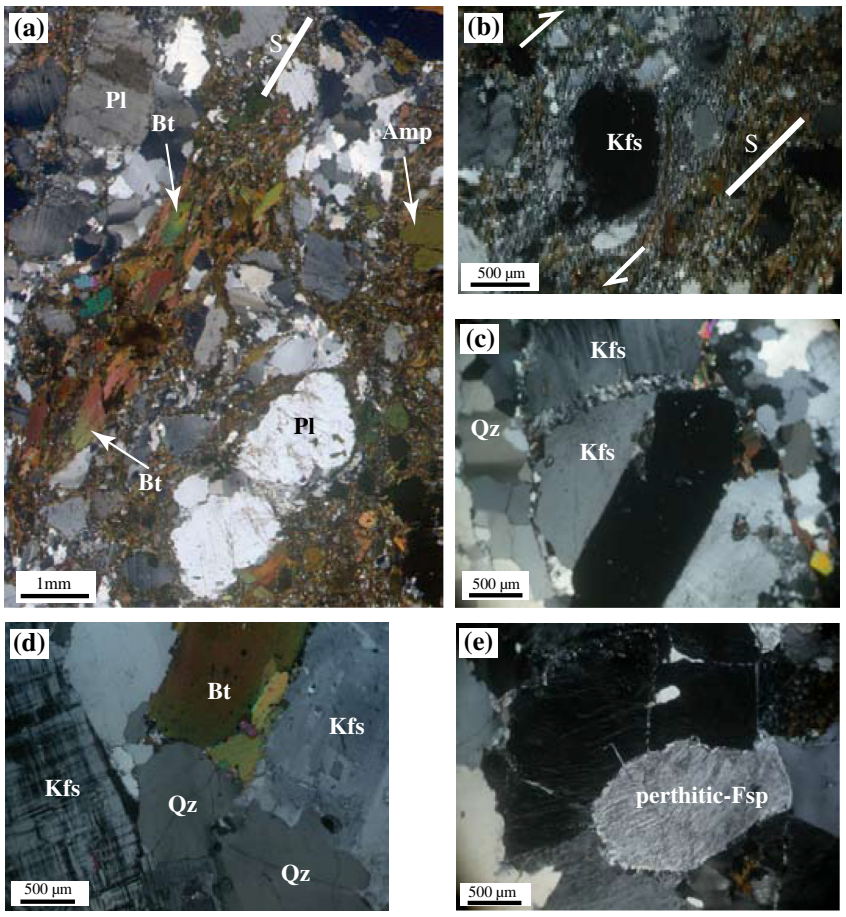

Fig. 4. Microstructural features of intrusions. (a) Foliated porphyritic coarse-grained quartz-monzonite of Dassa intrusion with fragmented K-feldspars; (b) pressure shadow on a feldspar phenoclast and recrystallization tails in the Dassa intrusion indicating dextral shear sense; (c) microfractures in K-feldspars phenocrysts filled by small grains of quartz and feldspar in the Tré granite; (d) Igneous texture in the Gobada granite; (e) fine-grained quartz and feldspars crystallizing along microfractures of perthitic feldspar grains in the Fita granite. The half arrows indicate the shearing sense; the lines indicate the trace of the foliation (S).

Monzonite and quartz-monzonite are mostly composed of andesine, biotite, quartz and amphibole. Most common accessory phases of different facies are epidote, titanite, zircon, ilmenite and magnetite in the Gobada intrusion. The MME within granite contain biotite, plagioclase (andesine) quartz and additional amphibole in enclaves from monzonite and quartz-monzonite.

Microstructural observations of granites, monzonites and quartz-monzonites show euhedral to subhedral feldspars that are sometimes affected by brittle fractures filled by quartz or quartz and feldspars assemblages (Fig. 4c). This suggests sub-solidus crystallization of residual melts (Bouchez et al., 1992; Vernon et al., 2004). In these rocks quartz is generally anhedral and biotite appears as elongated clusters (Fig. 4d). Late discrete minor shear bands characterized by fine-grained feldspar, quartz and mica may be observed in the Tré intrusion.

Most of the microstructures observed in the Tré, Gobada and Tchetti intrusions are magmatic and there is no evidence that these granitoids have undergone solid-state ductile deformation. However a weak brittle deformation can be recognized in the rocks of Tré intrusion indicating sub-solidus deformation at lower temperatures.

3.2.2.2. Petrography of the Fita intrusion. The Fita intrusion (Fig. 2) consists of an equigranular medium grained alkaline granite cross-cut by metric-scale dykes of microgranite and rhyolite. The granite and related dykes of microgranites are composed of quartz, perthitic feldspars, biotite, chlorite, apatite, titanite, epidote, fluorine, magnetite, ilmenite and pyrite. The microgranite as well as the rhyolite contain K-feldspar and quartz phenocrysts. The fine-grained mesostase of the microgranite is made of quartz, K-feldspars and biotite.

The microstructures observed in the Fita granite are comparable to those in the Tré, Gobada and Tchetti granitoids. Feldspars are euhedral to subhedral, sometimes subdivided into few large grains (Fig. 4e). Quartz is anhedral; biotite and magnetite occur as agglomerates. These microstructural features suggest that the Fita granite preserves a magmatic fabric. But locally the northern margin of the Fita granite is affected by a later low-temperature brittle deformation. In the related microfractures, crystallization of chlorite after biotite together with epidote, quartz and magnetite is associated with a late hydrothermal fluid circulation.

3.2.2.3. Summary of granite petrography. Field observations and microstructural investigations show that only Dassa is oriented and deformed at solid state in amphibolite facies metamorphic conditions. The other intrusions (Tré, Gobada, Tchetti and Fita) appear to be undeformed in the field, and microstructural analysis clearly indicates magmatic textures (Figs. 3 and 4). The Dassa, Tré, Gobada and Tchetti rock types are two feldspars granites while Fita is only K-feldspar bearing. All granites contain MME (Fig. 3) suggesting a magmatic mingling between granitic magma and a more mafic magma.

Table 1
Whole-rock chemical major and trace elements composition of Dassa, Tré, Gobada, Tchetti and Fita granitoids; normalization of major elements to 100% in anhydrous basis; qM: quartz-monzonite, G: granite, Mz: monzonite, mD: monzodiorite, (*) granitic dykes of Tré in the Dassa intrusion, (*) microgranular mafic enclave.

Intrusions	Dassa			Tré				Gobada				Tchetti		Fita	
Sample	BE14	BE61	BE06	BE10	BE11	BE12	BE09	BE26	BE25	BE24	BE22	BE40	BE41	BE54	BE55
Type	qM	G	G*	mD**	Mz	G	G	mD**	qM	G	G	G	G	G	G
SiO_2 (%)	62.82	71.04	70.82	55.82	61.16	71.12	71.97	55.32	65.27	72.00	74.96	70.5	71.46	73.48	74.97
TiO_2	1.2	0.51	0.51	2.99	1.43	0.53	0.43	1.49	0.77	0.35	0.2	0.24	0.19	0.22	0.22
Al_2O_3	15.66	13.73	13.63	14.07	15.13	13.76	14.06	16.71	16.27	14.37	13.77	14.17	13.63	13.31	12.86
Fe_2O_3	6.25	3.6	3.45	12.91	8.11	3.42	2.27	8.54	4.15	2.4	1.13	2.36	1.69	2.61	2.02
MnO	0.07	0.04	0.05	0.17	0.11	0.04	0.03	0.11	0.05	0.04	0.03	0.05	0.04	0.04	0.04
MgO	1.77	0.47	0.43	2.12	1.38	0.51	0.44	3.24	1.19	0.43	0.19	0.37	0.37	0.07	0.03
CaO	4.14	1.81	1.63	5.08	4.19	1.64	1.38	5.84	2.68	1.36	0.79	1.23	1.11	0.59	0.68
Na_2O	3.42	3.08	3.49	2.74	3.39	2.8	3.14	4.23	3.95	3.62	3.79	5.7	6.35	3.88	3.73
K_2O	4.27	5.61	5.82	3.27	4.53	6.02	6.12	3.71	5.41	5.31	5.09	5.24	5.07	5.77	5.41
P_2O_5	0.35	0.13	0.18	0.83	0.55	0.18	0.14	0.77	0.28	0.1	0.04	0.11	0.1	0.02	0.01
SUM	100	100	100	100	100	100	100	100	100	100	100	100	100	100	100
Ni (ppm)	11.1	6.1	7.3	9.9	8.2	5.4	5.5	22.7	8.7	7.7	6.9	4.8	4.1	10.9	11.1
Cu	2	0	0	18	8.6	0	0	24	0	0	0	0	0	0	0
Zn	81.7	56	61.7	142.8	113.8	63.3	52.1	95.3	53.6	39.8	19.5	43.2	33.2	95	85.3
Ga	15.1	15.2	15.6	16.4	18.3	14.9	14.4	15.7	14.9	13.6	13.4	14.4	13.9	22.6	19.5
Rb	95.9	186	206.2	81.7	155.6	231.2	248.3	121.9	161.9	239.3	307.6	188.4	186.3	191.3	228.3
Sr	402.7	183.5	158.4	405.1	385.7	183.4	152.6	700.5	308.8	149.3	97.8	152.3	129.9	22	21.5
Y	44.1	35.1	40.9	50.7	50.8	22.9	22.8	32.3	21.1	33.9	26.4	24.7	22.8	95.7	98.4
Zr	510.6	359	331.4	421.8	679.4	353.7	263	424	405.4	236.6	105.3	324.3	209	575.6	354.7
Nb	29.3	25.5	27.2	46.8	57.7	19.8	18.9	39	22.3	28.3	37.1	33.9	28.9	63.4	49
Ta	1.8	1.6	1.7	2.9	3.6	1.2	1.2	2.4	1.4	1.8	2.3	2.1	1.8	4	3.1
Pb	15	23.1	22.7	11.9	20.1	21.1	30.8	14.1	19.1	22.4	27.1	30.7	32.7	24.8	46.1
Sn	0	0	0	0	0	0	0	0	0	0	0	0	0	1.2	2.7
Th	8.7	32.3	36	6	20.3	39.5	45.1	9.2	31.3	22.7	33.7	19	24.3	18	22.9
U	0	1.3	1.7	0	2.1	1.3	1.4	0	2.4	4.3	8.4	3.4	3.2	2.4	3.9

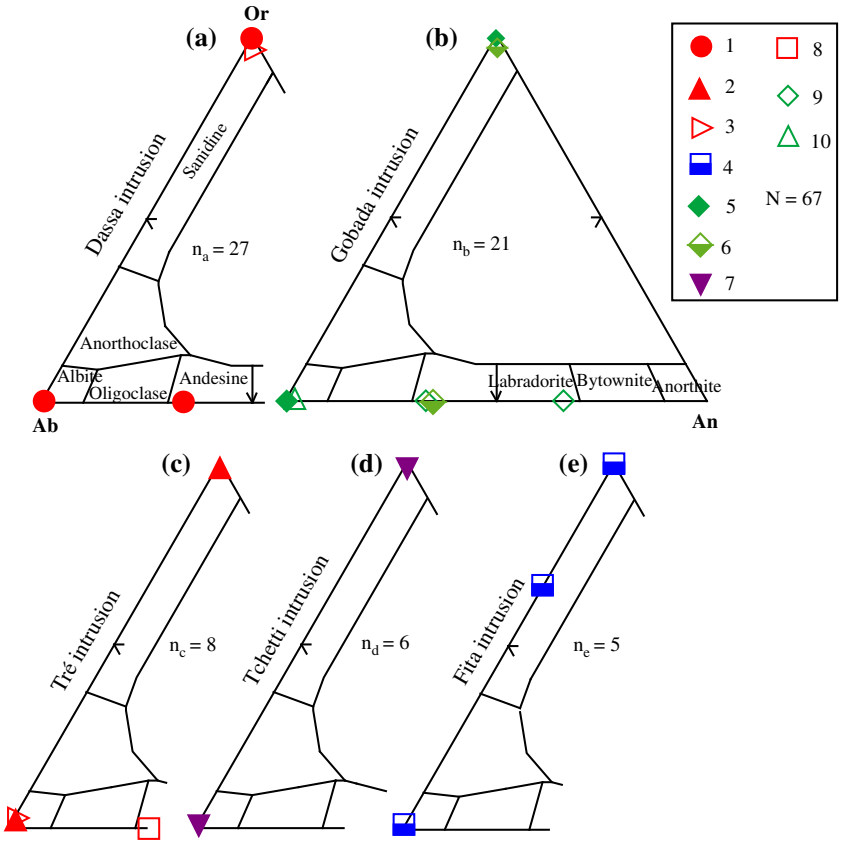

Fig. 5. Composition of feldspars from various granitoids (a–e). (1) Porphyritic coarse grained quartz-monzonite and monzonite of Dassa intrusion; (2) porphyritic medium grained granite of Tré intrusion; (3) dyke of porphyritic medium grained granite in the Dassa intrusion; (4) medium grained granite of the Fita intrusion; (5) coarse grained granite of the Gobada intrusion; (6) porphyritic quartz-monzonite of the Gobada intrusion; (7) fine to medium grained granite of the Tchetti intrusion; (8) enclave of monzodiorite in the porphyritic coarse grained monzonite of the Tré intrusion; (9) enclave of monzodiorite in the quartz-monzonite of the Gobada intrusion; (10) mafic microgranular enclave in the granite of the Gobada intrusion; N: total number of analyses.

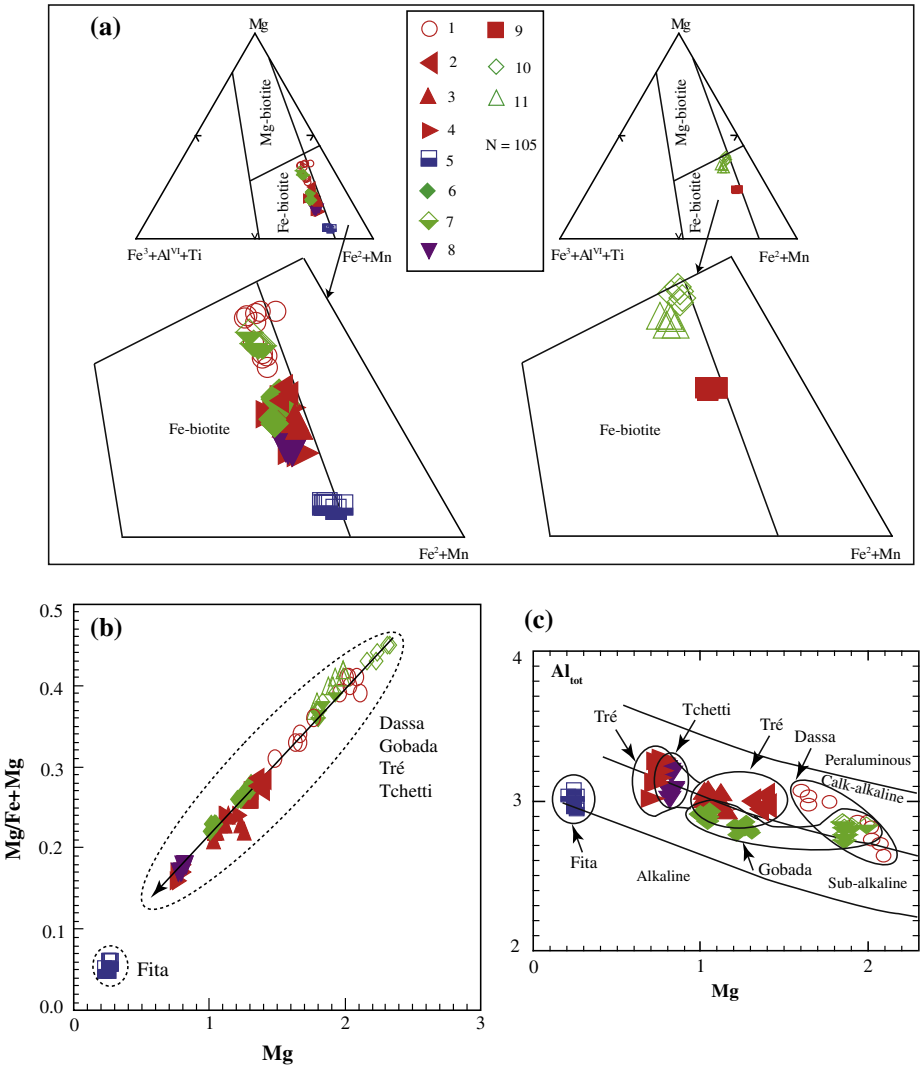

Fig. 6. Composition of biotites from studied granitoids. (a) Classification of biotites after Foster (1960); (b) Mg number (Mg/Fe + Mg) vs. Mg of biotite; (c) typology of magmas from biotite after Nachit et al. (1985); (1) porphyritic coarse-grained granite and quartz-monzonite of Dassa; (2) porphyritic monzonite of the Tré intrusion; (3) porphyritic medium-grained granite of the Tré intrusion; (4) dyke of porphyritic medium grained of Tré granite in the Dassa intrusion; (5) medium grained granite of the Fita intrusion; (6) coarse grained granite of the Gobada intrusion; (7) porphyritic quartz-monzonite of the Gobada intrusion; (8) fine to medium grained granite of the Tchetti intrusion; (9) enclave of monzodiorite in the porphyritic grained monzonite of the Tré intrusion; (10) enclave of monzodiorite in the Gobada intrusion quartz-monzonite; (11) mafic microgranular enclave in the granite of the Gobada intrusion; N: total number of analyses.

4. Mineralogy and chemistry

Field and petrographic data highlight the diversity of the granites spatially related to the KSZ. In order to characterize them more precisely, and to compare the different granite intrusions, we have completed preliminary geochemical studies on the analysis of minerals and whole-rocks.

4.1. Analytical procedures

Mineral analyses were performed at Laboratoire Magmas and Volcans (LMV), Clermont-Ferrand (France) using a Cameca SX-100 electron microprobe. Calculations of feldspar, biotite and amphibole structural formulae were based on 32 (O), 24 (O) and 23 (O) respectively.

Whole rock and trace elements compositions (Table 1) were analyzed by X-ray fluorescence (XRF) spectrometry at the Ecole Nationale des Mines, Saint-Etienne (France) using a Siemens SRS 3400 spectrometer (WDS, rhodium target X-ray tube, 60 kV). Detection limits for trace elements are the order of ppm. Concentration of tantalum (Ta) has been determined from the niobium (Nb) content using the (Nb/Ta) ratio = 16 (Rudnick and Fountain, 1995). Geochemical diagrams in this paper were generated using GCDkit 3.0 package (Janoušek et al., 2006).

4.2. Mineral chemistry

Most of the granitoids contain both orthoclase (Or_{95-100}) and plagioclase; the later shows albite (Ab_{95-100}) and andesine (An_{30-33}) composition in Dassa, Tré and Gobada. In the more differentiated granite of Tchetti plagioclase consists only in albite (Fig. 5). These two feldspars granitoids probably derive from high-K calk-alkaline magmas.

The Fita granite differs from other granitoids by the occurrence of perthitic sanidine ($Or_{66-67}Ab_{33-34}$) and the abundance of K-feldspar (Fig. 5e). This suggests a different parent magma with alkaline affinity where crystallization of sanidine at high temperature was followed by demixing during cooling.

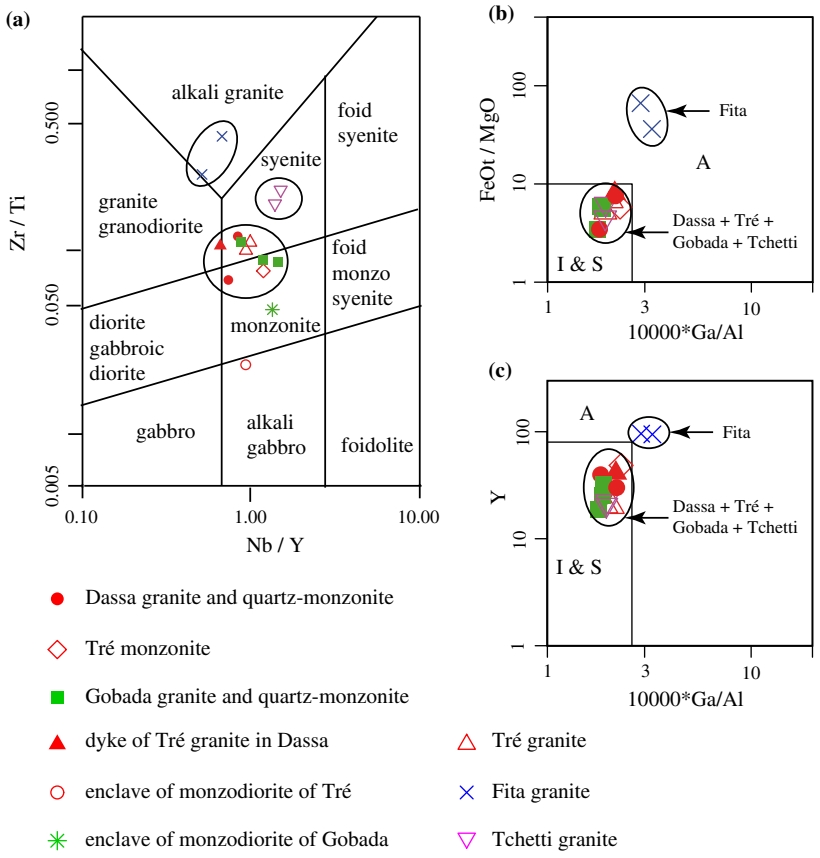

Fig. 7. Geochemical discrimination diagrams for granitoids Dassa, Tré, Gobada, Tchetti and Fita intrusions. (a) Nb/Y vs. Zr/Ti diagram (modified after Pearce, 1996); (b and c) FeOt/MgO vs. 10,000°Ga/Al and Y vs. 10,000°Ga/Al diagrams of Whalen et al. (1987).

In the ternary chemical classification diagram of Foster (1960) (Fig. 6a), biotite plots within the Fe-biotite area. However within X_{Mg} (X_{Mg} = mol. Mg/(Fe + Mg)) vs. Mg diagram (Fig. 6b) for biotite, biotite from Dassa, Tré, Gobada and Tchetti intrusions have higher X_{Mg} (>0.16) compared to that from Fita intrusion (<0.06).

In most of the intrusions, i.e. Dassa, Tré, Gobada and Tchetti, X_{Mg} of biotite is higher within monzodiorite, monzonite and quartz-monzonite than in granite. X_{Mg} ranges between 0.31 and 0.41 for the quartz-monzonite and granite of Dassa and 0.36–0.39 and 0.22–0.28, respectively for the quartz-monzonite and granite of Gobada. The X_{Mg} of biotite from the Tré monzonite and granite ranges respectively between 0.26–0.28 and 0.16–0.24 whereas X_{Mg} ranges between 0.17 and 0.18 in the Tchetti intrusion. Biotite within MME is quite similar to that of their host: X_{Mg} = 0.37–0.45 for Gobada and 0.26–0.27 for Tré intrusion. In Fita granite, biotite is characterized by a clear depletion in MgO with very low X_{Mg} varying between 0.05 and 0.06 (Fig. 6b).

The chemical features of biotite reveal that magmas of the Dassa, Gobada, Tré, Tchetti and Fita granitoids may not derive from a meta-sedimentary protolith. According to Nachit et al. (1985) (Fig. 6c), the Dassa, Gobada, Tré and Tchetti granitoids probably crystallize from calk-alkaline to sub-alkaline magma whereas the alkaline Fita granite was derived from lithospheric or asthenosphere mantle. This assumption fits well with the discrimination, based on the feldspar mineralogy, between the two feldspars granitoids group and the K-feldspar granite of Fita (Fig. 5).

4.3. Whole-rock major and trace elements chemistry

All the granitoid intrusions are characterized by high K_2O contents (Table 1) ranging between 4.3 and 5.6 wt% in Dassa intrusion, 4.5–6.1 wt% in Tré, 5–5.3 wt% in Gobada, about 5 % in the Tchetti and 5.4–5.6 wt% in Fita. Also, except the Tchetti granite which is clearly Na_2O richer (5.7–6.4 wt%), other granitoids display similar content in Na_2O from 2.7 to 3.9 wt%. Interestingly, the Fita granite shows lower CaO contents (0.6–0.7 wt%), MgO (0.0–0.1 wt%) and Sr (22 ppm) and is particularly enriched in HFSE such Y (96–98 ppm) and Nb (49–63 ppm).

Nb/Y vs. Zr/Ti diagram (Pearce 1996) (Fig. 7a) shows that samples from the Fita intrusion plot in the alkali granite while granites of Dassa, Tré, Tchetti and Gobada are in the sub-alkaline field.

All granitoids are ferroan type with high (FeO/FeO + MgO) ratio. However, the (FeO/FeO + MgO) ratio is nearly similar for the Dassa, Tré, Gobada, Tchetti intrusions (between 0.73 and 0.85) close to that of the enclaves (Tré, Gobada). Again, the Fita granite stands out by its higher (FeO/FeO + MgO) value ranging between 0.96 and 0.98.

Granites from Dassa, Tré, Gobada, Tchetti and Fita are clearly metaluminous with alumina saturation index (ASI) ranging from 0.76 to 0.98. This suggests that magmas of all granites are partially hybridized and derived from mingling and chemical-exchange mixing of magmas from crustal and mantle sources.

It is worth noting that in the Whalen et al. (1987) discrimination diagram (Fig. 7b and c), the Dassa, Tré, Gobada and Tchetti granites plot in the I and S-type fields (calk-alkaline, metaluminous to peraluminous). The Fita granite is an exception and plots in the A-type granite field.

Our preliminary geochemical study supports and extends the chemical discrimination previously proposed by Bigiorggero et al. (1988) between high-K calk-alkaline suite which are well represented in this study (Dassa, Tré, Gobada, Tchetti) and in contrast to the more alkaline intrusion at Fita. This is in good agreement with a post-collisional geodynamic setting.

Table 2
AMS parameters of Dassa, Tré, Gobada, Tchetti and Fita intrusions and host metamorphic rocks of the Kandi Shear Zone in Centre-Bénin. km, mean susceptibility (10^{-3} SI); P', corrected anisotropy degree; T, shape parameter; K_1 and K_3 are, respectively, the magnetic lineation and the pole of the magnetic foliation. $\alpha K_{1,3}$ is the semi-angle (measured in degrees) of confidence ellipses around K_1 and K_3 axes.

Site	Lon (E)	Lat (N)	Km	P'	T	K_1			K_3		
	(°)	(°)	(mSI)			Dec	Inc	αK_1	Dec	Inc	αK_3
Dassa intrusion											
3	2.198	7.746	0.24	1.08	0.250	349	16	9	253	21	6
5	2.186	7.78	0.2	1.15	0.62	10	25	9	264	31	5
6	2.189	7.762	0.27	1.08	0.013	355	9	5	261	22	8
13	2.245	7.771	1.67	1.12	−0.334	355	19	7	244	47	23
14	2.254	7.779	0.47	1.06	−0.408	346	13	9	103	67	15
16	2.222	7.809	0.52	1.08	0.109	355	44	8	240	23	8
18	2.306	7.84	0.49	1.06	0.253	184	7	18	87	45	11
19	2.307	7.853	0.51	1.09	0.312	195	11	5	95	45	4
69	2.185	7.795	0.49	1.18	0.774	5	17	5	271	15	5
70	2.186	7.822	0.32	1.17	0.883	170	26	5	274	27	2
71	2.204	7.859	0.25	1.1	0.566	356	22	6	260	15	3
Tré intrusion											
1	2.202	7.719	0.08	1.12	0.478	354	10	5	260	21	2
2	2.2	7.727	0.19	1.04	−0.030	328	27	45	237	3	44
7	2.192	7.725	0.23	1.09	−0.094	5	38	27	253	26	12
8	2.201	7.716	0.18	1.08	0.156	345	9	3	253	15	5
9	2.195	7.72	0.12	1.09	−0.176	350	22	4	243	34	6
12	2.201	7.717	0.37	1.07	0.342	353	14	16	86	12	38
10	2.191	7.717	0.45	1.07	−0.015	350	17	6	260	1	9
Gobada intrusion											
20	2.01	7.802	0.78	1.06	0.077	147	1	25	53	83	30
21	2.012	7.803	1.04	1.04	0.105	245	33	29	60	57	19
22	2.012	7.805	0.83	1.05	0.471	0	6	63	111	73	35
23	2.012	7.792	0.16	1.01	0.166	188	35	25	300	29	18
24	2.014	7.793	0.08	1.02	0.533	33	45	28	286	16	38
25	2.018	7.801	0.20	1.03	−0.541	219	20	33	110	41	36
26	2.018	7.803	0.20	1.03	0.039	12	1	53	282	8	40
27	2.014	7.788	1.82	1.04	−0.105	315	16	35	59	42	43
29	2.016	7.783	0.16	1.01	−0.541	9	44	23	183	46	34
30	2.006	7.763	0.13	1.01	−0.63	39	49	14	237	39	34
32	2.014	7.768	0.16	1.02	0.277	296	60	15	141	27	15
33	2.022	7.782	0.14	1.02	0.214	243	60	25	111	22	38
34	2.028	7.79	0.06	1.01	−0.101	301	24	47	209	5	27
Tchetti intrusion											
47	1.664	7.828	0.13	1.08	0.544	35	36	19	287	23	2
48	1.663	7.838	0.11	1.04	0.272	115	64	5	299	26	5
49	1.663	7.846	0.11	1.08	0.078	54	45	4	295	21	6
50	1.663	7.82	0.12	1.05	0.442	18	16	15	286	9	6
51	1.669	7.824	0.10	1.06	0.746	23	6	20	291	23	4
52	1.66	7.83	0.12	1.05	0.469	22	27	5	281	21	5
Fita intrusion											
64	2.128	7.683	0.21	1.02	0.441	4	67	20	96	1	16
65	2.123	7.678	6.92	1.19	0.235	35	26	2	291	26	4
66	2.109	7.67	4.18	1.08	−0.499	5	31	6	274	1	19
67	2.114	7.675	5.30	1.04	−0.072	36	15	6	236	74	6
68	2.109	7.676	9.05	1.06	0.078	28	47	28	285	12	39
Host rocks											
4	2.2	7.772	0.33	1.12	0.011	1	7	4	92	5	6
17	2.232	7.816	0.33	1.13	0.541	349	21	4	236	45	5
39	2.081	7.891	0.31	1.07	−0.06	16	11	4	280	29	7
54	1.756	7.856	0.35	1.08	0.09	332	15	14	237	17	10
58	1.969	7.922	0.28	1.17	0.719	9	17	14	276	9	4
60	2.039	7.906	0.30	1.09	−0.649	13	26	7	279	8	43
56	1.826	7.873	16.13	1.18	−0.402	327	10	8	67	40	21
37	2.055	7.842	16.35	1.67	−0.248	16	2	11	106	3	11

5. AMS investigation

5.1. Sampling and AMS determination

50 Sites were sampled within the KSZ for AMS investigation: 11 from Dassa, 7 from Tré, 13 from Gobada, 6 from Tchetti, 5 from Fita and 8 in various gneisses of basement. The difficulties of access to sites and the density of the vegetation were limits for a regular sampling and explain the uncovered areas mainly for the Gobada, Tchetti and Fita intrusions. For each sampling site, two 25-mm-diameter oriented cores were collected using a gasoline-powered drill. They have been orientated with respect to geographic North and the horizontal plane using solar sightings and a magnetic compass equipped with a clinometer. Oriented cores have been cut into two or three 22-mm-long specimens, providing an average of five specimens per site.

AMS measurements was performed on 260 specimens at the Laboratoire Magmas et Volcans, Saint Etienne (France) using a

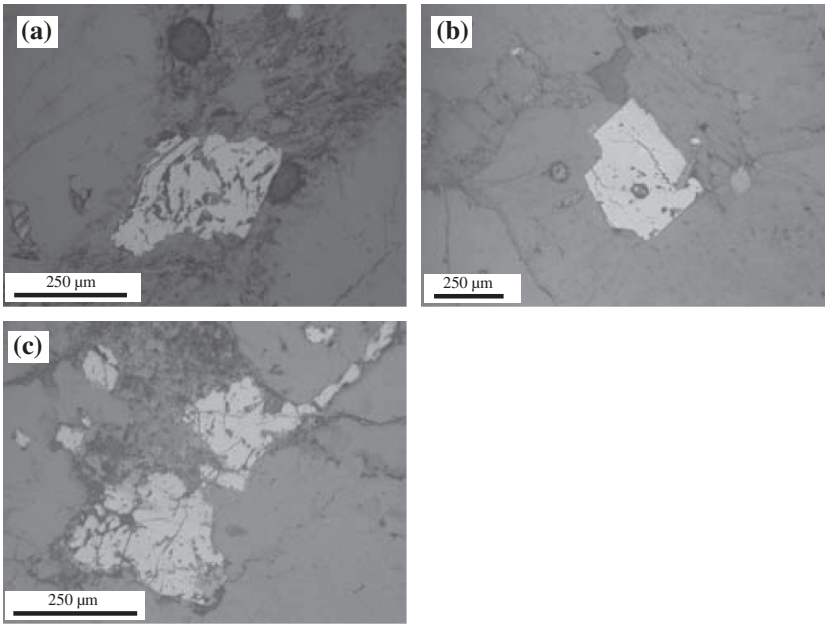

Fig. 8. Photomicrographs (reflected light) of magnetite grains from granitoids: (a) magnetite within the foliation of Dassa quartz-monzonite; (b) igneous euhedral magnetite in the Gobada granite; (c) igneous magnetite in the Fita granite.

Kappabridge instrument, MFK1-FA model (AGICO, Czech Republic). Resulting dataset for each specimen provides information on the orientation (declination and inclination) of the three principal orthogonal axes of the AMS ellipsoid ($k_1 \geqslant k_2 \geqslant k_3$) and on scalar data such the bulk magnetic susceptibility K_m, the corrected anisotropy degree P' (Jelinek, 1981) and the shape parameter T of the AMS ellipsoid, respectively expressed as:

$$K_m = (k_1 + k_2 + k_3)/3$$

$$P' = \exp\left[2(\ln k_1 - \ln K_m)^2 + 2(\ln k_2 - \ln K_m)^2 + 2(\ln k_3 - \ln K_m)^2\right]^{1/2}$$

$$T = (2\ln k_2 - \ln k_1 - \ln k_3)/(\ln k_1 - \ln k_3)$$

The T parameter ranges from −1 (prolate ellipsoid) to +1 (oblate ellipsoid). The average orientation of AMS ellipsoid axes for the five specimens of each sampling site (K_1, K_2 and K_3) and their 95% confidence angles was determined using Jelinek's statistics from the ANISOFT 42 package programs. The AMS data are reported in Table 2.

Magnetic mineralogy was determined through reflected light observations, microprobe analyses and thermomagnetic measurements (K–T curves) at low and high temperature using a cryostat apparatus (CS-L) and a furnace (CS-4) under Ar atmosphere coupled to the MFK1-FA instrument. The low temperature measurements range from −192 °C to room temperature and the high temperature measurements were performed from room temperature to 700 °C (heating cycle) and back (cooling cycle).

5.2. Magnetic mineralogy

Microscopic examination and microprobe analyses from all sampled granites reveal the presence of paramagnetic minerals such as biotite and amphibole in the Dassa and Tré intrusions. Opaque minerals such as ilmenite and magnetite in the five intrusions. Ilmenite is dominant in the Dassa, Tré, Gobada and Tchetti intrusions. Ilmenite is subhedral to anhedral and appears as single isolated grains, associated with biotite clusters or enclosed in amphibole and plagioclase porphyroclasts. Ilmenite later recrystallized into titanite. Magnetite is observed in the Dassa quartz-monzonites, in the Gobada and Fita granites (Fig. 8a and b). In the Dassa intrusion, magnetite grains are weakly elongated within the foliation whereas they are euhedral in the Gobada granite. In the Fita granite, the opaque mineralogy is dominated by ubiquitous interstitial grains suggesting the magnetite late crystallization (Fig. 8c).

In the host metamorphic rocks of intrusions, reflected light microscope observations show commonly the occurrence of both ilmenite and magnetite. But the mafic amphibole ± biotite ± garnet ± pyroxene gneiss contains mainly magnetite as opaque minerals.

Thermomagnetic analyses were carried on the different samples in order to precisely define the magnetic mineralogy (Fig. 9). Samples from Dassa, Gobada and Fita intrusions show two distinct thermomagnetic curves at low and high temperatures. The first ones display Verwey transition at −160 °C and typical reversal curves with Curie temperature of 580 °C indicating the presence of pure magnetite in some sites (Fig. 9a–c) while the second curves with weak magnetic susceptibility variation and regular decreasing (Fig. 9d–f) indicate a prominent paramagnetic signature. This clearly demonstrates the heterogeneous distribution of magnetite in the Dassa, Gobada and Fita intrusions. The Tré and Tchetti intrusions (Fig. 9g and h) present the characteristics of paramagnetic granitoids.

These different approaches demonstrate that both paramagnetic minerals (biotite and amphibole) and ferromagnetic minerals (large Ti-poor magnetite) are the carriers of the magnetic fabric in Dassa, Gobada and Fita intrusions. In contrast, in the Tré and Tchetti intrusions, the paramagnetic signal dominates the magnetic susceptibility and therefore paramagnetic minerals (biotite ± amphibole) are the main carriers of the magnetic fabric.

5.3. Anisotropy of low-field magnetic susceptibility (AMS)

5.3.1. Scalar data

For the Dassa and Gobada granitoids the bulk magnetic susceptibility ranges from 0.18 to 2.16 mSI and 0.04–2.53 mSI, respectively. Low magnetic susceptibility values (km < 0.50 mSI) are

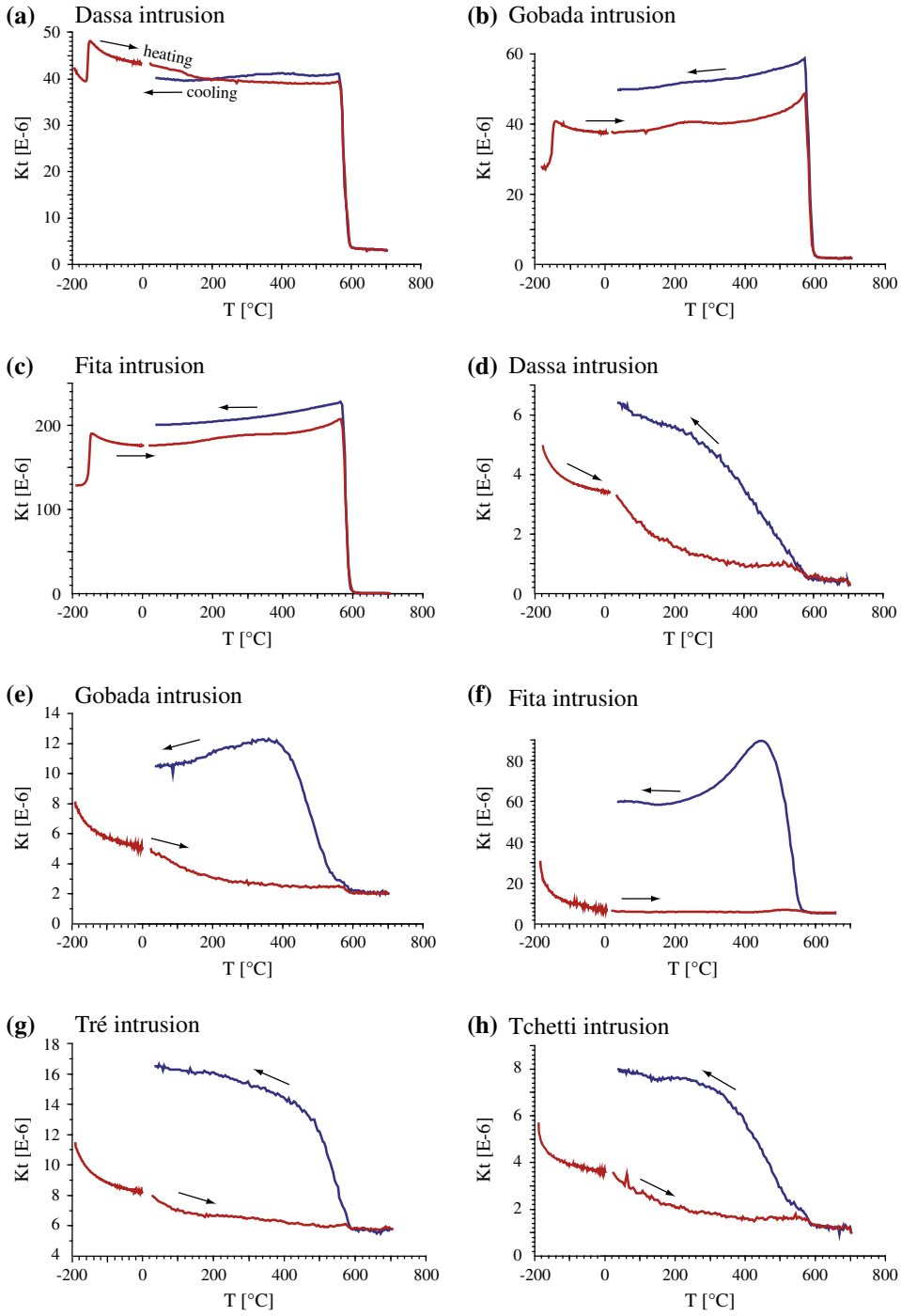

Fig. 9. Thermomagnetic curves of samples from the intrusions; (a–c) ferromagnetic samples with magnetite; (d–h) paramagnetic samples. For the latter, the thermomagnetic curves are not reversible because of mineralogical transformations and apparition of new magnetic phases during heating.

prevailing that is mainly explained by both dominant paramagnetic minerals (69% and 72%, respectively for Dassa and Gobada specimens) and by a subordinate contribution of ferromagnetic minerals (Fig. 10a and b). Tré and Tchetti granitoids display the lowermost bulk magnetic susceptibility. It ranges from 0.07 to 0.78 mSI (with 94% of specimens having km < 0.50 mSI) and 0.09–0.14 mSI, respectively (Fig. 10c and d) in agreement with magnetic mineralogy consisting of paramagnetic minerals. In contrast, the Fita granite (Fig. 10e) presents the highest values of the bulk magnetic susceptibility ranging from 0.17 to 14.8 mSI. In this intrusion, high magnetic susceptibilities values (>0.50 mSI) are found in 80% of specimens and suggest an important contribution of magnetite to the measured magnetic susceptibility.

The bulk magnetic susceptibility in the host metamorphic rocks of the intrusions is lower than 0.50 mSI in the two pyroxenes gneiss, garnet-biotite gneiss, garnet-biotite ± sillimanite ± cordierite gneiss and migmatites. On the opposite, the amphibole–biotite gneiss presents a bulk magnetic susceptibility value higher than 0.50 mSI and ranging from 3.57 to 30.60 mSI.

Corrected anisotropy degree (P') and shape of AMS ellipsoids (T) for intrusions and their host rocks are presented in Fig. 11. The anisotropy degree of all specimens varies from 1.04 to 1.21 in

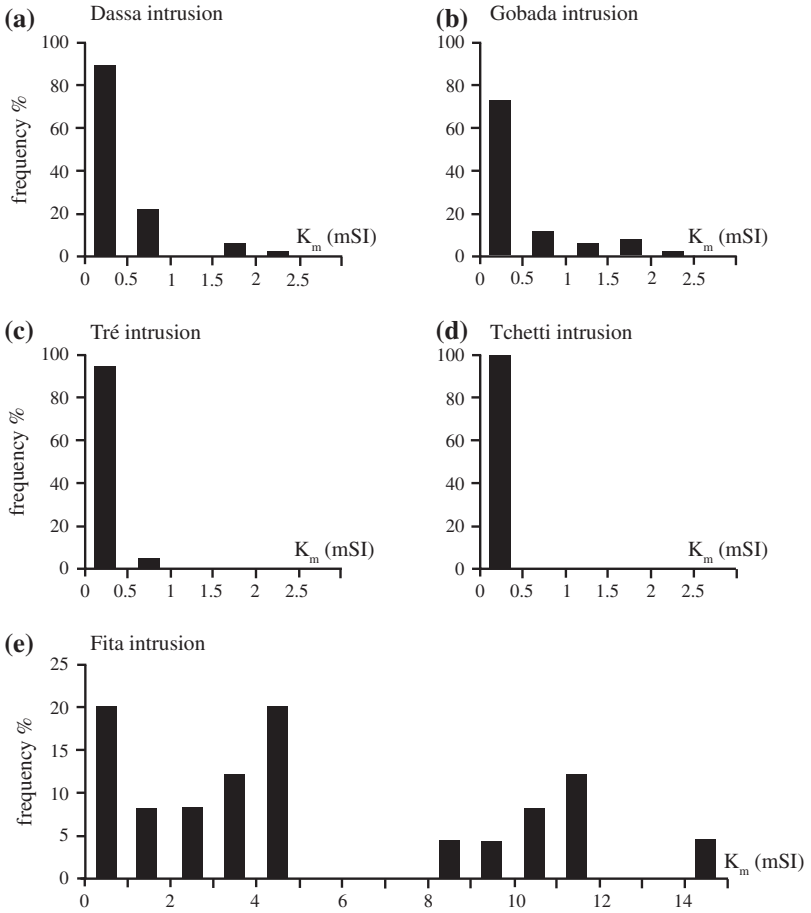

Fig. 10. Frequency histograms of bulk magnetic susceptibility (km) from all measured specimens of the various intrusions.

the Dassa granites and quartz-monzonites and the *T* values of specimens range from −0.71 to 0.92 (Fig. 11a). In the Dassa intrusion, 75% of specimens have an oblate shape ($T > 0$). In addition the specimens with the highest anisotropy ($P' > 1.10$) are strongly oblate ($T > 0.5$). These P' and *T* values are related to the intense solid-state deformation of the Dassa intrusion. In the Tré intrusion, P' ranges from 1.08 to 1.15 (Fig. 11b) and the oblate specimens in the granite ($T > 0$) are about 70%. Tchetti and Gobada intrusions have a lower anisotropy degree ranging from 1.04 to 1.11 and 1.01 to 1.18 respectively (Fig. 11c and d). For these intrusions, *T* value ranges from −0.04 to 0.91 and −0.71 to 0.88 (Fig. 11c and d) and 97% and 49% of specimens have oblate shape respectively. For Gobada intrusion, signatures of paramagnetic and ferromagnetic specimens were separated (Fig. 11d). P' is lower for paramagnetic specimens than for ferromagnetic ones and *T* values show indifferently oblate and prolate shapes. In Fita intrusion, P' ranges from 1.02 to 1.23, *T* varies from −0.69 to 0.79 (Fig. 11e) and about 44% of specimens have an oblate shape. Such high P' values (about 1.2) are related to the ferromagnetic specimens which present oblate or triaxial ($T \approx 0$) AMS ellipsoids.

In host metamorphic rocks, the corrected anisotropy degree ranges from 1.04 to 1.82 and the AMS ellipsoids are oblate as well as prolate.

5.3.2. Magnetic foliations and lineations

All the poles of the magnetic foliations (K_3 axes) and the magnetic lineations (K_1 axes) are plotted on the lower-hemisphere, equal-area projections (Fig. 12) and data are reported in Table 2. Maps of the AMS foliations and lineations are presented in Fig. 13. The K_1 and K_3 axes of the magnetic susceptibility ellipsoids for the Dassa, Tré, Tchetti and Fita intrusions are well clustered in contrast to that observed for the Gobada pluton.

The magnetic foliations in the Dassa intrusion (Figs. 12 and 13a) dip moderately to steeply in most sites, and strike N–S in the eastern and western branches, and NNE–SSW in the central branch of the intrusion. Magnetic lineations are dominantly N–S trending with gentle North or South plunging. Magnetic foliations in Tré intrusion (Figs. 12 and 13b) are steeply dipping and trend N–S. Magnetic lineations plunge gently northwards. The Tchetti intrusion (Figs. 12 and 13c) is characterized by well-grouped magnetic foliations with a NNE–SSW orientation and a steep dip to the East. Magnetic lineations are distributed along a girdle perpendicular to K_3. In Gobada intrusion, the K_1 and K_3 axes of magnetic susceptibility ellipsoids are more scattered than in others intrusions (Fig. 12d). If paramagnetic and ferromagnetic fabrics are considered separately, they give two significantly distinct directions. Mean magnetic foliation carried by paramagnetic specimens has a steep dip trending NNE–SSW whereas that given by ferromagnetic specimens is NNW–SSE oriented with a gentle dip. Mean magnetic lineations show a gentle plunge for both paramagnetic and ferromagnetic specimens but display contrasted directions, close to the N for the former and close to the NW for the latter. So, magnetic fabric of the Gobada intrusion is composite. It is worth noting that although paramagnetic fabric is less pronounced than ferromagnetic fabric, it is nevertheless consistent in direction with magmatic schlierens observed in the field.

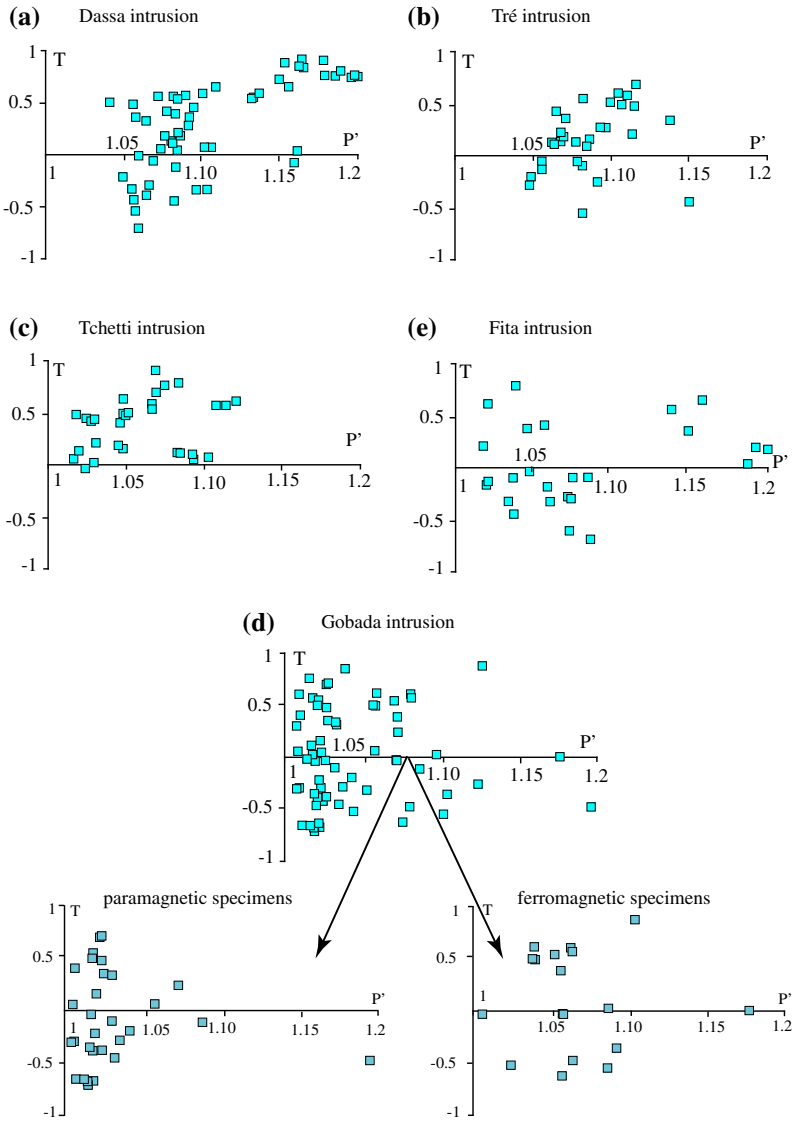

Fig. 11. Relationship between the corrected anisotropy degree P′ and the shape of AMS ellipsoids (T parameter) from all measured specimens of the various intrusions.

Magnetic foliations of the Fita intrusion (Figs. 12 and 13e) strike generally NNE–SSW with a steep to vertical dip. Magnetic lineations trend N–S for sites located on the margins of the intrusion, and NE–SW plunging to the North with a gentle to steep dip for sites located inside the intrusion.

The magnetic fabric of the host gneisses is generally parallel to the foliation measured in the field. The magnetic foliation (Fig. 12f) strikes generally NNW to NNE (mean orientation N 03°) with steep dip (mean dip 83°). The magnetic lineation displays gentle plunge (mean plunging 10° N) with sub-meridian orientation (mean orientation N 04°).

6. Discussion

6.1. Nature and structure of the granitoids

As demonstrated above, types of granitoids can be distinguished in regard of their petrological and microstructural characteristics. Such characteristics are reliable markers to understand the tectonic setting of the petrogenesis of granitic bodies associated to the KSZ. Thus these results provide evidence to better constrain the geodynamic evolution of the KSZ in the central Bénin region.

6.1.1. Nature of granitic magmas

As attested by their chemical composition and magmatic mineralogical assemblages, Dassa, Tré, Gobada and Tchetti plutonic rocks derived from high-K calk-alkaline magmas. All of these granites are ferroan, metaluminous I- and S-types. Observations of numerous MME within granitic intrusions, of xenocrystals exchange as well as chemical transfers between MME and hosts suggest a possible hybridization through magmatic mingling between magmas produced from both crustal and mantle sources. In contrast to the other plutons, Fita is an alkaline intrusion (Bessoles and Trompette, 1980; Bigiorggero et al., 1988; Kalsbeek et al., 2012; Adissin Glodji, 2012), characterized by annitic, Mg-depleted, biotite and by crystallization of only K-feldspar. Fita's whole rock chemistry is also marked by high (FeOt/MgO), K_2O, Zr, Y, Nb contents and low LIL/HFS elements ratios and low CaO, MgO and Al_2O_3 values. This is in good agreement with an A-type granite affinity.

6.1.2. Microstructures and magnetic fabrics

AMS measurements reveal well-marked magnetic fabrics in most intrusions contradicting field apparent isotropy. Only the Gobada intrusion presents a nearly isotropic magnetic fabric, which results from the combination of two distinct fabrics carried

by paramagnetic and ferromagnetic samples, respectively. Within the gneissic basement, magnetic foliation and lineation from paramagnetic samples show a relatively good correlation with both field and AMS measurements. Microstructural analyses indicate different origins for the fabrics: solid-state deformation or magmatic flow related. The Dassa intrusion is the only one to clearly show evidence of solid-state deformation. It is also characterized by high anisotropy values ($P' > 10\%$). Tectonic and magnetic foliations are consistent with that the regional tectono-structural pattern. Deformation and dynamic recrystallization of the Dassa intrusion occurred under amphibolite facies conditions. In contrast to the Dassa intrusion, the Tré, Tchetti, Gobada and Fita intrusions show evidences for magmatic flow fabrics. The magnetic foliation measured in Tré, Tchetti, Gobada (paramagnetic samples) strikes ~N–S and dips steep to vertical, and therefore agrees fairly well with foliations observed in the gneisses. Only the magnetic foliations of Gobada determined, from ferromagnetic measurements, strongly differ. Such a divergence with the regional tectonic pattern is not yet fully understood. However, the study of the magnetic mineralogy seems to exclude the presence of secondary ferromagnetic minerals resulting from hydrothermal alteration. Furthermore, there is no correlation between location of the samples within the intrusion, and distribution of paramagnetic and ferromagnetic properties. Magnetic lineation shows a more heterogeneous distribution than magnetic foliation. The lineation is sub-horizontal in the Tré granite whereas it is girdle distributed in the Tchetti granite.

Magnetic fabrics of the Fita intrusion can be distinguished from others by steep and vertical dips, N–S to NNE–SSW trending foliation and the lineations, which are shifted to the NNE with higher plunge relative to the Tré and Gobada intrusions.

6.2. Evolution of granitic magmatism and relative chronology of intrusions

Petrological, chemical and structural investigations completed on granitoids from central Bénin (Bénin-Nigerian Shield) reveal (i) the ante- and syn-tectonic chronology of intrusions relative to the KSZ activity and (ii) the intrusion of two types of magmas, high-K calk-alkaline (Dassa, Tré, Gobada and Tchetti) and alkaline (Fita). In this area, the porphyritic coarse-grained granite and quartz-monzonite in the Dassa intrusion were emplaced before the N–S trending strike-slip tectonics and were deformed and transformed into orthogneiss. The ductile deformation observed in the Dassa intrusion is also confirmed by the high value of anisotropy degree revealed by the AMS measurements.

High-K calk-alkaline magmatism keeps going during strike-slip movement along the KSZ as exemplified by the emplacement of Tré, Tchetti and Gobada granites. These intrusions emplaced after the solid-state deformation of Dassa intrusion, as testified by the occurrence of enclaves of Dassa orthogneiss in the Tré granite. The synchronous character of emplacement of these 3 intrusions (i.e. Tré, Tchetti and Gobada) with regards to the KSZ activity is highlighted by the preservation of magmatic textures but also by the development of steep to vertical dip and sub-meridian trending magmatic foliation. Geometry of the magmatic foliation is consistent with the stress field responsible for the mylonitic foliation in the country rocks gneisses.

The Fita intrusion presents structural and petrological differences from the other granitoids: magmatic fabrics with a different geometry and alkaline signature. The observed NNE orientation of the magnetic foliation is similar to the foliation of the low-temperature tectonite bands located at the East and West of the intrusion. This suggests that the Fita intrusion was intruded to a shallower crustal level than the other intrusions. Moreover, the Fita intrusion is spatially associated with the Idaho-Mahou volcano-sedimentary basin (Boussari, 1975; Breda, 1989) and its chemistry is closely similar to that of alkaline rhyolites found in the basin (Adissin Glodji, 2012). So we assume the subvolcanic environment for the Fita intrusion as contemporaneous to the opening of the basin and therefore to the late stage of the KSZ Ediacaran activity. Moreover, the A-type affinity of the Fita granite also argues for a shallow depth crustal emplacement of the intrusion as suggested by Bonin (2007).

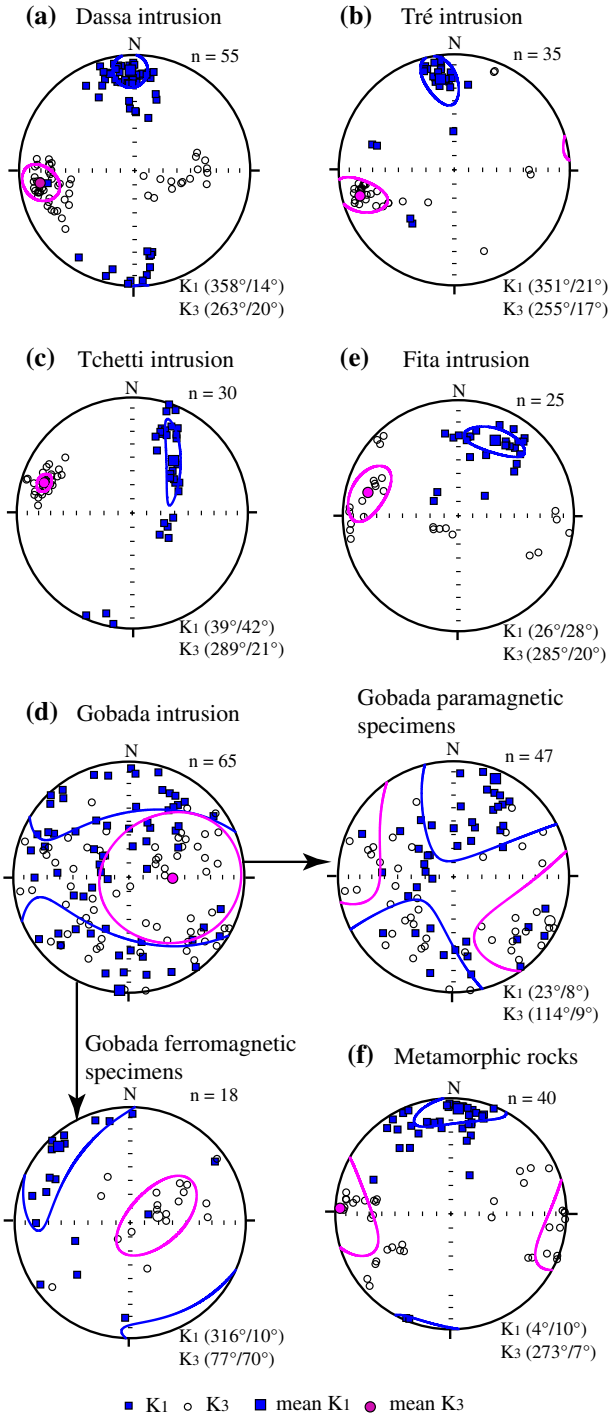

Fig. 12. Lower hemisphere, equal-area stereographic projections of the two principal axes of AMS ellipsoids (K_1 and K_3) of all specimens of intrusions and host rocks; *n* = number of specimens. N indicates the geographic North.

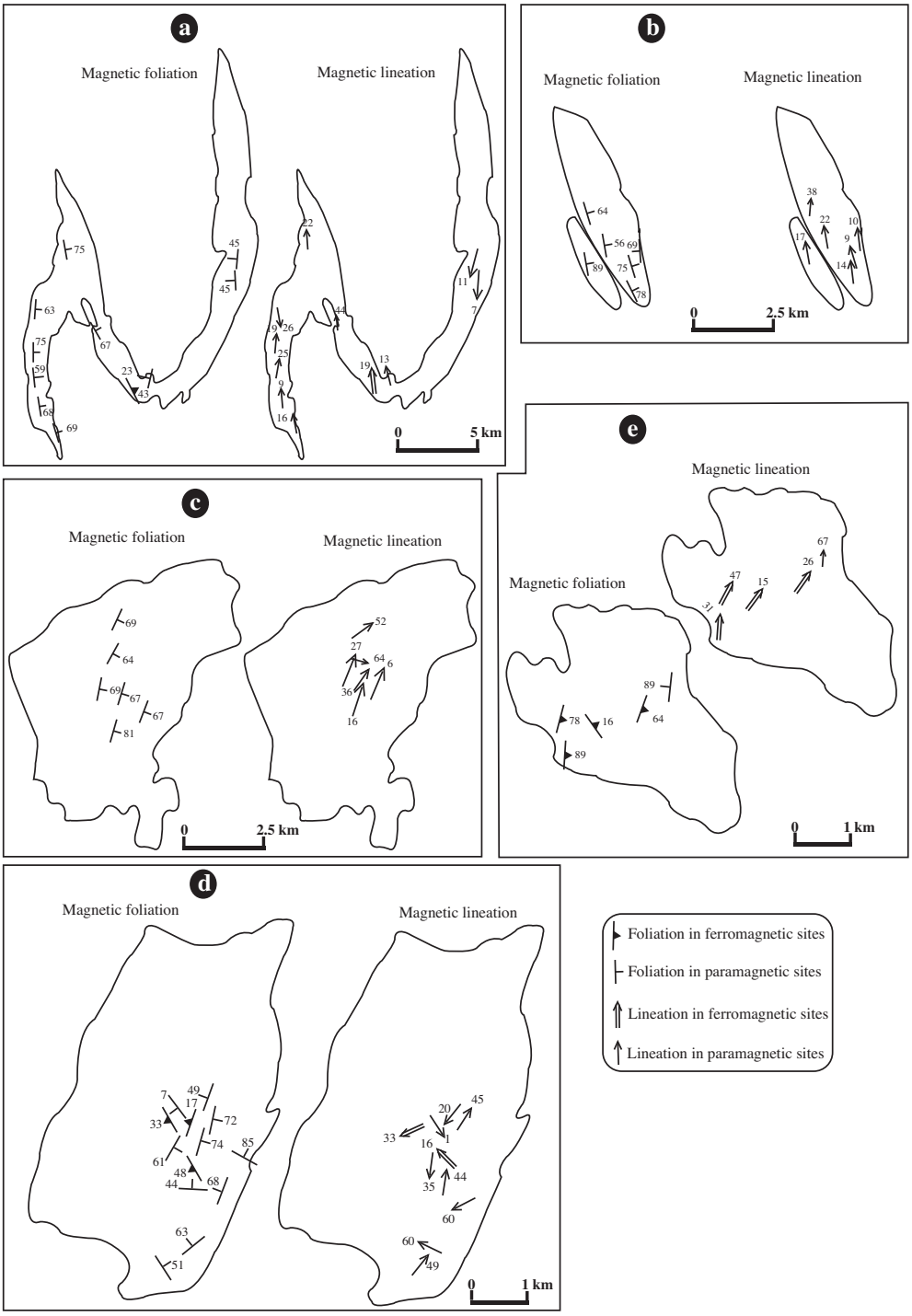

Fig. 13. Maps of magnetic structures (foliations and lineations) (a) Dassa, (b) Tré, (c) Tchetti, (d) Gobada and (e) Fita intrusions.

6.3. Structural and regional implications

Structural mapping from field and AMS studies of the KSZ metamorphic rocks reveal vertical foliation and horizontal lineation suggesting a dominant transcurrent regime. No vertical lineation has been observed or measured in the KSZ area. Nevertheless, magnitudes and shapes of magnetic fabrics could provide further information on strain (e.g., Borradaile, 1988).

In the Dassa and Tré intrusions, the magnetic lineation axes (K_1) and the pole of the foliation (K_3) are well-clustered and sub-parallel to magnetic lineation and foliation measured in metamorphic rocks. Such magnetic fabrics are similar to those observed in transcurrent shear zones (Egydio-Silva et al., 2005). The authors also correlate variations of the magnetic AMS fabrics with variations in strain regime. Well-defined magnetic foliation and girdle forming lineation, as for example observed in the Tchetti intrusion, could reflect the effect of locally stronger axial compression. However correlation of AMS patterns with strain is not straightforward and the distribution in girdle of magnetic lineations in the Tchetti intrusion may be also due to the shape of the biotite, which is the main magnetic fabric carrier. In this latter hypothesis, because of their oblate shape, biotite is a poor marker of the magnetic

lineation. However, we note that the Tré paramagnetic fabric, located in the eastern side of the KSZ, is strikingly different from that measured in Tchetti intrusion. This emphasizes the effect of strain regime variation across the KSZ.

There is also observed a repartition of the shape of AMS ellipsoids in the granitoid intrusions across the KSZ. In the Tchetti intrusion, which is located at the West of the KSZ, the AMS ellipsoids are exclusively oblate whereas those from the Tré pluton, located to the East of the KSZ, are oblate and prolate. Such repartition of the shape of AMS ellipsoids in the granitoid intrusions could be related to variations in magnetic-mineralogy content as well as contrasted strain regimes across the KSZ. In the paramagnetic granites, the relationship between the anisotropic properties of micas and the shape of the AMS ellipsoids are well established by several studies (Tarling and Hrouda, 1993; Bouchez, 2000; Borradaile and Jackson, 2010 and references therein). In granites without magnetite, the oblateness shape of biotite makes the form of AMS ellipsoids planar as observed in the Tchetti granite. However, measurement of both oblate and prolate AMS ellipsoids in the paramagnetic syn-kinematic granitoids of Tré suggests that the exclusively oblate shape of AMS ellipsoids measured in Tchetti might not be linked only to the shape of biotite but also reflects an axial compression signature associated to strain partitioning across the KSZ. It also highlights the transpressive character of the KSZ, which has also been observed in other Pan-African/Brasiliano orogenic belts such as the Kaoko in Namibia (Goscombe and Gray, 2008) or the Ribeira in southeastern Brazil (Egydio-Silva et al., 2005).

The emplacement of an alkaline pluton postdates the evolution of the post-collisional high-K calc-alcaline series. Such magmatic evolution is also documented for the late-Pan-African orogeny in the Hoggar (Algeria) and Adrar des Iforas in Mali (Liégeois, 1987; Bonin, 1990; Black and Liégeois, 1993) that are the northern equivalents of the Dahomeyides belt. Also the Fita alkaline magma is similar in composition with the Meruoca pluton emplaced along the Transbrasiliano lineament in the NE Brazil (Archanjo et al., 2009).

A recent chemical and geochronological study of some granites in the Bénin basement, including the Fita granite, considered that they start being emplaced in an active continental margin setting (Kalsbeek et al., 2012). Our results show that the emplacement of the studied granitoids, except Dassa, is geometrically and chronologically related to the KSZ, which is considered as part of a late orogenic intracontinental shear zone (Caby, 1989; Trompette, 1994; Neves, 2003; Arthaud et al., 2008; Dos Santos et al., 2008). Thus, the high-K calk-alkaline and alkaline intrusions are not specific for an active continental margin setting and continue being emplaced in a late-orogenic environment.

7. Conclusion

The central Bénin region is a good example of time and space relationships between magmatism and shear zone activity. Taking into account microstructures analyses and AMS structures together with magmas compositions allow one to define relative chronology between magmatism and the Kandi Shear Zone (KSZ) late Ediacaran activity.

- An early high-K calk-alkaline magmatic event (Dassa intrusion) predates the transcurrent tectonics.
- The transcurrent activity of the Kandi Shear Zone starts by the deformation of the porphyritic coarse-grained granites and quartz-monzonites of the Dassa intrusion into orthogneiss. The Kandi Shear Zone activity continues as the Tré, Gobada, Tchetti and Fita emplace. The former syn-kinematic intrusions (Tré, Gobada and Tchetti) crystallized from high-K calk-alkaline magmas and are classic I- and S-types granitoids whereas Fita was sourced from alkaline magma.
- The A-type Fita evolved in a sub-volcanic environment in close relation with the opening of the Idaho-Mahou basin and probably represents one the latest magmatic events.

These results highlight the similarities between the Kandi Shear Zone in central Bénin and the mega-shear zones observed in Hoggar, in Mali and in North-East Brazil (Liégeois, 1987; Bonin, 1990; Black and Liégeois, 1993; Nouar et al., 2011; Vauchez et al., 1995; Neves, 2003; Archanjo et al., 2009). However, radiometric dating is required to more precisely constrain the geodynamic evolution of the western Dahomeyides in Bénin.

Acknowledgements

This study was supported by the French Ministry of Foreign Affairs (MAE) through a PhD grand to LAG and additional supports from the Rhône-Alpes region (CMIRA program) and from the Ministry of Mines of Bénin. We thank C. Guilbaud, J.L. Devidal and F. Gallice for analytical and technical assistance, and Peter Bowden for discussions and suggestions. We also thank C.J. Archanjo and an anonymous reviewer for their very useful remarks.

References

Adissin Glodji, L., 2012. La zone de cisaillement de Kandi et le magmatisme associé dans la région de Savalou-Dassa (Bénin): étude structurale, pétrologique et géochronologique, Thèse de doctorat, Université Jean Monnet Saint-Etienne (France) et Université d'Abomey-Calavi (Bénin), 260p.

Affaton, P., Rahaman, M.A., Trompette, R., Sougy, J., 1991. The dahomeyide orogen: tectonothermal evolution and relationships with the volta basin. In: Dallmeyer, R.D., Lécorché, J.P. (Eds.), The West African Orogens and Circum-Atlantic Correlatives. Springer-Verlag, Berlin, pp. 107–122.

Ajibade, A.C., Wright, J.B., 1989. The Togo-Benin-Nigeria Shield: evidence of crustal aggregation in the Pan-African belt. Tectonophysics 165, 125–129.

Archanjo, C.J., da Silva, E.R., Caby, R., 1999. Magnetic fabric and pluton emplacement in a transpressive shear zone system: the Itaporanga porphyritic granitic pluton (northeast Brazil). Tectonophysics 312, 331–345.

Archanjo, C.J., Hollanda, M.H.B.M., Rodrigues, S.W.O., B.B. Neves, B., Armstrong, R., 2008. Fabrics of pre- and syntectonic granite plutons and chronology of shear zones in the Eastern Borborema Province, NE Brazil. J. Struct. Geol. 30, 310–326.

Archanjo, C.J., Launeau, P., Hollanda, M.H.B.M., Macedo, J.W.P., Liu, D., 2009. Scattering of magnetic fabrics in the Cambrian alkaline granite of Meruoca (Ceará state, northeastern Brazil). Int. J. Earth Sci. (Geol. Rundsch) 98, 1793–1807.

Arthaud, M.H., Caby, R., Fuck, A., Dantas, E.L., Parente, C.V., 2008. Geology of the northern Borborema Province, NE Brazil and its correlation with Nigeria, NW Africa. In: Pankhurst, R.J., Trouw, R.A.J., Brito Neves, B.B., De Wit, M.J. (Eds.), West Gondwana: Pre-Cenozoic Correlations Across the South Atlantic Region. Geological Society, London, Special Publications, 294, pp. 49–67.

Attoh, K., Samson, S., Agbossoumondé, Y., Nude, P.M., Morgan, J., 2013. Geochemical characteristics and U-Pb zircon LA-ICPMS ages of granitoids from the Pan-African Dahomeyide orogen, West Africa. J. Afr. Earth Sci. 79, 1–9.

Bessoles, B., Trompette, R., 1980. Géologie de l'Afrique: La chaine panafricaine: « zone mobile d'Afrique centrale (partie sud) et zone mobile soudanaise », B.R.G.M., Orléans, France, 397p.

Bigiorggero, B., Boriani, A., Cadoppi, P., Sacchi, R., Vedogbéton, N., Yevidé, H., 1988. Données préliminaires sur les granites du Bénin Meridional. Rendiconti della Società Italiana di Mineralogica e Petrologia 43, 477–484.

Black, R., Liégeois, J.P., 1993. Cratons, mobile belts, alkaline rocks and continental lithospheric mantle: the Pan-African testimony. J. Geol. Soc. Lond. 150, 89–98.

Bonin, B., 1990. From orogenic to anorogenic settings: evolution of granitoid suites after a major orogenesis. Geol. J. 25, 261–270.

Bonin, B., 2007. A-type granites and related rocks: evolution of a concept, problems and prospects. Lithos 97, 1–29.

Borradaile, G.J., 1988. Magnetic susceptibility, petrofabrics and strain. Tectonophysics 156, 1–20.

Borradaile, G.J., Jackson, M., 2010. Structural geology, petrofabrics and magnetic fabrics (AMS, AARM, AIRM). J. Struct. Geol. 32, 1519–1551.

Bouchez, J.-L., 2000. Anisotropie de susceptibilité magnétique et fabrique des granites. Comptes Rendus de l'Académie des Sciences, Paris 330, 1–14.

Bouchez, J.L., Delas, C., Gleizes, G., Nédélec, A., Cuney, M., 1992. Submagmatic microfractures in granites. Geology 20, 35–38.

Boussari, W.T., 1975. Contribution à l'étude géologique du socle cristallin de la zone mobile Pan-Africaine (Région centrale du Dahomey), Thèse de Doctorat, Université de Besançon, 105p.

Boussari, W., Rollet, M., 1974. Découverte d'un bassin volcano-sédimentaire dans la région Centre-Ouest du Dahomey. Comptes Rendus Académie des Sciences, Paris 279, 29–32.
Breda, 1985. Etude de la cartographie géologique et prospection minière de reconnaissance au Sud du 9ème parallèle. Première phase, 111p.
Breda, 1989. Notice explicative de la carte géologique à 1/200000. Feuilles Pira-Savè, Abomey-Zagnanado, Lokossa-Porto-Novo, 77p.
Caby, R., 1989. Precambrian terranes of Benin-Nigeria and Northeast Brazil and the late Proterozoic South Atlantic fit. Geol. Soc. Am. Special Paper 230, 145–158.
Caby, R., 2003. Terrane assembly and geodynamic evolution of central-western Hoggar: a synthesis. J. Afr. Earth Sci. 37, 133–159.
Caby, R., Sial, A.N., Arthaud, M.H., Vauchez, A., 1991. Crustal evolution and the Brasiliano Orogeny in Nort-east Brazil. In: Dallmeyer, R.D., Lécorché, J.P. (Eds.), The West African Orogens and Circum-Atlantic Correlatives. Springer, Berlin, pp. 373–397.
Caen-Vachette, M., 1975. Age pan-africain des granites de Sinendé, Savè et Fita (Dahomey). Comptes Rendus Académie des Sciences, Paris 281, 1793–1795.
Castaing, C., Triboulet, C., Feybesse, J.L., Chèvremont, P., 1993. Tectonometamorphic evolution of the Ghana, Togo and Benin in the light of the Pan-African/Brasiliano orogeny. Tectonophysics 218, 323–342.
Dada, S.S., 2008. Proterozoic evolution of the Nigeria-Borborema province. In: Pankhurst, R.J., Trouw, R.A.J., Brito Neves, B.B., De Wit, M.J. (Eds.), West Gondwana: Pre-Cenozoic Correlations Across the South Atlantic Region, Geological Society, London, Special Publications, 294, pp. 121–136.
Dawaï, D., Bouchez, J.-L., Paquette, J.-L., Tchameni, R., 2013. The Pan-African quartz-syenite of Guider (north-Cameroon): magnetic fabric and U–Pb dating of a late-orogenic emplacement. Precambr. Res. 236, 132–144.
Déléris, J., Nédélec, A., Ferré, E., Gleizes, G., Ménot, R.P., Obasi, C.K., Bouchez, J.L., 1996. The Pan-African Toro Complex (northern Nigeria): magmatic interactions and structures in a bimodal intrusion. Geol. Mag. 133, 535–552.
Djouadi, M.T., Gleizes, G., Ferré, E., Bouchez, J.L., Caby, R., Lesquer, A., 1997. Oblique magmatic structures of two epizonal granite plutons, Hoggar, Algeria: late-orogenic emplacement in a transcurrent orogen. Tectonophysics 279, 351–374.
Dos Santos, T.J.S., Fetter, A.H., Neto, J.A.N., 2008. Comparisons between the northwestern Borborema Province, NE Brazil, and the southwestern Pharusian Dahomey Belt, SW Central Africa. Geol. Soc. Lond. Special Publications 294, 101–120.
Egydio-Silva, M., Vauchez, A., Raposo, M.I.B., Bascou, J., Uhlein, A., 2005. Deformation regime variations in an arcuate transpressional orogen (Ribeira belt, SE Brazil) imaged by anisotropy of magnetic susceptibility in granulites. J. Struct. Geol. 27, 1750–1764.
Ferré, E., Gleizes, G., Bouchez, J.L., Nnabo, P.N., 1995. Internal fabric and strike-slip emplacement of the Pan-African granite of Solli Hills, northern Nigeria. Tectonics 14, 1205–1219.
Ferré, E., Gleizes, G., Djouadi, M.T., Bouchez, J.L., Ugodulunwa, F.X.O., 1997. Drainage and emplacement of magmas along an inclined transcurrent shear zone: petrophysical evidence from a granite-charnockite pluton (Rahama, Nigeria). In: Bouchez, J.L., Hutton, D.H.W., Stephens, W.E. (Eds.), Granite: From Segregation of Melt to Emplacement Fabrics. Petrology and Structural Geology. Kluwer Publishing Co., Dordrecht, pp. 253–273.
Foster, M.D., 1960. Interpretation of the Composition of Trioctahedral Micas. U.S. Geological Survey of Professional Paper, 354-B, pp. 11–40.
Goscombe, B.D., Gray, D.R., 2008. Structure and strain variation at mid-crustal levels in a transpressional orogen: a review of Kaoko Belt structure and the character of West Gondwana amalgamation and dispersal. Gondwana Res. 13, 45–85.
Guiraud, R., Alidou, S., 1981. La faille de Kandi (Bénin), témoin du rejeu fini-crétacé d'un accident majeur à l'échelle de la plaque africaine. Comptes Rendus de l'Académie des Sciences, Paris 293, 779–782.
Henry, B., Bayou, B., Derder, M.E.M., Djellit, H., Ouabadi, A., Khaldi, A., Hemmi, A., 2007. Late Panafrican evolution of the main Hoggar fault zones: implications of magnetic fabric study in the In Telloukh pluton (Tin Serririne basin, Algeria). J. Afr. Earth Sci. 49, 211–221.
Henry, B., Liégeois, J.P., Nouar, O., Derder, M.E.M., Bayou, B., Bruguier, O., Ouabadi, A., Belhai, D., Amenna, M., Hemmi, A., Ayache, M., 2009. Repeated granitoid intrusions during the Neoproterozoic along the western boundary of the Saharan metacraton, eastern Hoggar, Tuareg shield, Algeria: an AMS and U–Pb zircon age study. Tectonophysics 474, 417–434.
Janoušek, V., Farrow, C.M., Erban, V., 2006. Technical note. Interpretation of whole-rock geochemical data in igneous geochemistry: introducing geochemical data Toolkit (GCDkit). J. Petrol. 47, 1255–1259.
Jelinek, V., 1981. Characterization of the magnetic fabric of rocks. Tectonophysics 79, 63–67.
Kalsbeek, F., Affaton, P., Ekwueme, B., Frei, R., Thrane, K., 2012. Geochronology of granitoid and metasedimentary rocks from Togo and Benin, West Africa: comparisons with NE Brazil. Precambr. Res. 196–197, 218–233.
Konaté, M. 1996. Evolution tectono-sédimentaire du bassin paléozoïque de Kandi (Nord Bénin, Sud Niger). Un témoin de l'extension post-orogénique de la chaîne panafricaine. Thèse de doctorat, Université de Dijon, France, 489p.
Liégeois, J.P., 1987. Le batholite composite de l'Adrar des Iforas (Mali): géochimie et géochronologie d'une succession magmatique du calco-alcalin à l'alcalin dans le cadre de l'orogenèse pan-africaine, Thèse de doctorat, Université libre de Bruxelles, 335p.
Liégeois, J.P., Abdelsalam, M.G., Ennih, N., Ouabadi, A., 2013. Metacraton: nature, genesis and behavior. Gondwana Res. 23, 220–237.
Nachit, H., Razafimahefa, N., Stussi, J.M., Carron, J.P., 1985. Composition chimique des biotites et typologie magmatique des granitoïdes. Comptes Rendus Académie des Sciences, Paris 301, 813–818.
Neves, S.P., 2003. Proterozoic history of the Borborema province (NE Brazil): correlations with neighboring cratons and Pan-African belts and implications for the evolution of western Gondwana. Tectonics 22, 1031. http://dx.doi.org/10.1029/2001TC001352.
Neves, S.P., Vauchez, A., Archanjo, C.J., 1996. Shear-zone controlled magma emplacement or magma-assited nucleation of shear zone? Insights from northeast Brazil. Tectonophysics 262, 349–364.
Neves, S.P., Vauchez, A., Feraud, G., 2000. Tectono-thermal evolution, magma emplacement, and shear zone development in the Caruaru area (Borborema Province, NE Brazil). Precambr. Res. 99, 1–32.
Neves, S.P., Marianoa, G., Beltrão, B.A., Correia, P.B., 2005. Emplacement and deformation of the Cachoeirinha pluton (Borborema province, NE Brazil) inferred through petrostructural studies: constraints on regional strain fields. J. S. Am. Earth Sci. 19, 127–141.
Nouar, O., Henry, B., Liégeois, J.P., Derder, M.E.M., Bayou, B., Bruguier, O., Ouabadi, A., Amenna, M., Hemmia, A., Ayache, M., 2011. Eburnean and Pan-African granitoids and the Raghane mega-shear zone evolution: image analysis, U–Pb zircon age and AMS study in the Arokam Ténéré (Tuareg shield, Algeria). J. Afr. Earth Sci. 60, 133–152.
Nsifa, N.E., Tchaméni, R., Nédélec, A., Siqueira, R., Pouclet, A., Bascou, J., 2013. Structure and petrology of Pan-African nepheline syenites from the South West Cameroun; implication for their emplacement mode, petrogenesis and geodynamic significance. J. Afr. Earth Sci. 87, 44–58.
Pearce, J.A., 1996. Sources and setting of granitic rocks. Episodes 19, 120–125.
Rudnick, R.L., Fountain, D.M., 1995. Nature and composition of the continental crust: a lower crustal perspective. Rev. Geophys. 33, 267–309.
Tarling, D.H., Hrouda, F., 1993. The Magnetic Anisotropy of Rocks. Chapman and Hall, London, 217p.
Trompette, R., 1994. Geology of Western Gondwana (2000–500 Ma). Pan-African-Brasiliano Aggregation of South America and Africa. Balkema, Rotterdam, 350p.
Vauchez, A., Neves, S., Caby, R., Corsini, M., Egydio-Silva, M., Arthaud, M., Amaro, V., 1995. The Borborema shear zone system, NE Brazil. J. S. Am. Earth Sci. 8, 247–266.
Vernon, R.H., Johnson, S.E., Melis, E.A., 2004. Emplacement-related microstructures in the margin of a deformed pluton: the San José tonalite, Baja California, México. J. Struct. Geol. 26, 1867–1884.
Whalen, J.B., Currie, K.L., Chappell, B.W., 1987. A-type granites: geochemical characteristics, discrimination and petrogenesis. Contrib. Miner. Petrol. 95, 407–419.